# SUPERCRITICAL METHANE STORAGE AND TRANSPORT IN SINGLE-WALL CARBON NANOTUBES

A Thesis

by

RUI KOU

Submitted to the Office of Graduate and Professional Studies of
Texas A&M University
in partial fulfillment of the requirements for the degree of

MASTER OF SCIENCE

| | |
|---|---|
| Chair of Committee, | I. Yucel Akkutlu |
| Committee Members, | John Pantano |
| | Khoa Bui |
| Head of Department, | Daniel A. Hill |

August 2016

Major Subject: Petroleum Engineering

# ABSTRACT

Quantification of gas storage and transport in organic-rich shale is important in determining natural gas production rates and reserves. However, laboratory measurements are challenging, due to very tight nature of the rock, and have large uncertainties due to presence of multiple mechanisms of gas storage and transport at multiple scales. The emphasis of this thesis is on understanding of storage and transport mechanisms and their interplay inside organic nano-capillaries. An atomistic modeling and molecular simulation approach is presented in investigating supercritical methane behavior in model carbon nanotubes representing nano-capillary.

Equilibrium Monte Carlo simulations show a non-uniform methane density profile across the diameter of the capillary. The results show excess methane at the central portion of the capillary indicating deviations from Langmuir adsorption model. Amount of excess methane is dependent on the competition in between the fluid-wall and fluid-fluid interactions.

To study the transport behavior of methane in nano-capillary, we performed nonequilibrium Molecular Dynamics simulations based on a moving piston model. The piston model allows us to study steady-state transport across the diameter of nanotube in order to understand the effects of adsorbed methane on transport under reservoir conditions. The results show that the adsorbed phase is not only mobile but also contribute significantly to total mass flux. The contribution of the adsorbed-phase is

profound in smaller capillaries. Simulations of transport with different sizes of capillaries show that the adsorbed-phase transport velocity is independent of capillary size, but strongly dependent on the pressure drop across the capillary. This allows us to quantify the adsorbed-phase velocity into an adsorbed phase mobility factor.

ACKNOWLEDGEMENTS

I would like to thank my committee chair, Dr. I. Yucel Akkutlu, and my committee members Dr. John Pantano and Dr. Khoa Bui for their guidance and support throughout the course of this research. I would also like to thank Sansarng Riewchotisakul for his advice and support in creating the simulation models.

Thanks to my friends and colleagues in the Petroleum Engineering Department and to the faculty and staff for making my time at Texas A&M University a wonderful experience.

Finally, thanks to my wife and my parent for their encouragement that motivates me to pursue my graduate education.

NOMENCLATURE

| | |
|---|---|
| $A_{ads}$ | Cross section area for adsorbed phase transport, $m^2$ |
| $A_{dif}$ | Cross section area for diffusion transport, $m^2$ |
| $C$ | Concentration, $mol/m^3$ |
| $D_s$ | Adsorbed phase mobility, $nm^2/(psi \cdot ps)$ |
| $D$ | Diffusion coefficient, $m^2/s$ |
| $J_{vis}$ | Mass flux of viscous flow, $\frac{kg}{m^2 s}$ |
| $J_{total}$ | Total mass flux, $\frac{kg}{m^2 s}$ |
| $J_{dfs}$ | Molar flux by diffusion, $\frac{mol}{m^2 s}$ |
| $k$ | Intrinsic permeability, $m^2$ |
| $k_a$ | Apparent permeability, $m^2$ |
| $M_{CH4}$ | Molecular weight of methane, kg/mol |
| $M_{total}$ | Total mass transfer rate, kg/s |
| $M_{ads}$ | Adsorbed phase mass transfer rate, kg/s |
| $M_{dif}$ | Diffusion mass transfer rate, kg/s |
| $M_{vis}$ | Viscous flow mass transfer rate, kg/s |
| $M_{HP}$ | Mass transfer rate based on HP equation, kg/s |
| P | Pressure, psi |
| $Q_{ads}$ | Volume transfer rate of adsorbed phase, $m^3/s$ |
| $Q_{vis}$ | Volume transfer rate of viscous flow, $m^3/s$ |

| | |
|---|---|
| $r_{tube}$ | Radius of capillary, m |
| $r_{ads}$ | Radius of capillary excluding adsorbed phase, m |
| $r_{avg}$ | Average radius of capillary network, m |
| $R_{mf}$ | Mass flux ratio, dimensionless |
| $V_{ads}$ | Adsorbed phase velocity, nm/ps |
| $x$ | Distance in x direction, nm |
| $\rho_s$ | Adsorbed phase density, kg/m$^3$ |
| $\rho$ | Bulk phase density, kg/m$^3$ |
| $\mu$ | Viscousity, Pa·s |

TABLE OF CONTENTS

Page

LIST OF FIGURES

Page

LIST OF TABLES

Page

# 1. INTRODUCTION AND LITERATURE REVIEW

In general, it is considered that natural gas is stored and transported in resource shale in three types of pores at three different length scales: fractures, inorganic matrix pores, and organic pores (Akkutlu and Fathi, 2012; Wasaki and Akkutlu, 2015). Initial gas production is mainly due to fluid stored in large-scale fractures. At this early stage, contribution from the matrix is overwhelmed by compressed natural gas in fractures. After this initial production stage, the production rate drops to significantly lower levels, when gas transport and production from the matrix becomes rate-limiting. Although production rate due to transport in the matrix is significantly less than that in the fractures, the volume of fluid stored in the matrix is much larger and it sustains a longer period of a well's production life. Eventually, it contributes significantly to cumulative production. Hence, a better understanding of fluid storage and transport in the matrix would help to plan for a suitable production strategy to improve overall recovery from shale reservoirs.

Shown by SEM images of various shale samples (Wang and Reed 2009; Ambrose et al., 2012), the inorganic matrix pores are mostly slit shape and have larger dimensions compare to the organic pores. It is argued that the slit-shape geometry has been developed as a result of rock failure accompanied by cracking caused by fluid (pore) pressure in excess of hydrostatic pressure (Palciauskas and Domenico, 1980; Wasaki and Akkutlu, 2015). Mass transport at this scale is viscous-forces-controlled

flow, i.e., convection. This transport mechanism is characterized by a parabolic shape velocity profile. Description of the flow through the inorganic pore network can be done using conventional theory based on Darcy law. Permeability of inorganic matrix with slit-shape pores is stress sensitive. Various mechanistic models have been developed to describe the permeability. Wasaki and Akkutlu (2015) have recently suggested that the stress-sensitive permeability of the inorganic matrix can be modeled by Gangi's bed of nails model (Gangi, 1978)

The organic matter, widely known as kerogen, on the other hand, has pores that are mainly round shape. They are developed as a result of thermal maturation and conversion of kerogen into hydrocarbon fluids (Loucks et al., 2009). Using special imaging techniques, it has previously been shown that kerogen pores are interconnected and may include a network of small pores and capillaries with sizes typically less than 100 nm (Ambrose et al., 2012). Nano-size kerogen pores and capillaries are also known to have large capillary wall surface area which leads to significant physical adsorption. Because of its size and large surface area, fluid transport in kerogen pores could have non-continuum effects and pore-wall-dominated multi-scale effects, Kang et al. (2011); Akkutlu and Fathi (2012).

Direct measurement of quantities of nanoscale transport in kerogen is desirable but not practical with the currently available laboratory techniques. Instead, simulation techniques have been adopted to investigate pore scale transport. Lattice-Boltzmann-method (LBM) simulations of gas transport in organic capillaries smaller than 100nm

shows that transport could go through a transition in flow regime (Akkutlu and Fathi, 2012). The flow regime changes from viscous flow, which is characterized by parabolic shape velocity profile, to molecular (pore) diffusion, which maintains a uniform velocity profile at the central portion of the capillary. The same transition phenomenon can be described using the changes in the value of Knudsen number, a dimensionless number defined as the ratio of mean free path of molecules to the capillary diameter. Many researchers share the understanding that, with the pore diameter decreases (Knudsen number increases), viscous flow diminishes while diffusion-like flow becomes more pronounced. Hence, different types of diffusion-viscous flow models have been proposed covering both transport mechanisms and the transition-flow regime between them (Karniadakis et al. 2005; Sakhaee-Pour et al., 2012; Rahmanian, et al. 2013;Javadpour et al. 2009). A fundamental difference between these models is the treatment of mass flux contribution due to diffusion. Some models treat diffusion contribution as first and second order slip coefficients associated with Knudsen number (Beskok and Karniadakis 1999, Civan, F., 2010, Sakhaee-Pour and Bryant 2012**)** others consider diffusional flux as a separate mass flux term calculated by diffusion coefficients (Javadpour, F., 2009. Rahmanian, et al. 2013).

While the discussions on modeling pore diffusion in kerogen is ongoing, possibility of another transport mechanism associated with the adsorbed-phase transport has been considered. Kang et al. (2011), Fathi and Akkutlu (2012) argued the possibility of another transport mechanism appearing in organic capillaries. The authors compared

the adsorbed-phase transport to another well-dominated transport mechanism known as surface transport or surface diffusion. Surface diffusion had previously been considered for fluids under sub-critical condition, see, for example, the book by Do (1998). It is a continuous process of adsorbed fluid molecules hopping along the solid surface randomly between adsorption sites below the saturation pressure of the fluid. Each hopping movement requires a minimum activation energy, which is related to the isosteric adsorption heat. Driving force of surface diffusion is suggested to be chemical potential gradient, where in the case of single component methane flow, it can be simplified as adsorbed-phase density gradient (Fathi and Akkutlu, 2012). A molecular Dynamics (MD) simulations study of steady-state supercritical methane flowing through a 5nm diameter carbon nano-tube under reservoir pressure and temperature conditions has recently demonstrated the subtle differences between the adsorbed phase transport and the surface diffusion (Riewchotisakul and Akkutlu, 2015). Another nonequilibrium MD simulation based on a different computational methodology (using external force field) showed similar results and gave new insights into surface roughness effect on the surface diffusion(Feng and Akkutlu, 2015).

The objective of this research is to study the nature of transport of supercritical methane flowing through nano-size capillary. We are in particular interested in identifying the mechanisms and the transitions between the mechanisms. Using MD simulation, a steady-state flow system is developed with an upstream tank and a downstream tank providing constant pressure gradient. Simulation output file provides

the trajectories (i.e., locations and velocities) of each methane molecule. By analyzing methane density distribution and velocity profile across the diameter of the tube and analyzing the mass fluxes, signatures of each of the three transport mechanisms, namely, viscous flow (or convection), diffusion and adsorbed phase transport, are analyzed. Considering viscous effect during natural gas transport in kerogen pores could be negligible, a diffusion-surface diffusion dominated transport model could be proposed. Such a transport model should include an adjustment to a size-dependent kerogen permeability. In section 1.1, we start our literature review by comparing different gas adsorption theories. This is necessary for the reader to visualize a heterogeneous pore space, where free fluid and adsorbed fluid locations are separated.

## 1.1 Gas Adsorption Theories

In terms of hydrocarbon accumulation, a significant portion of hydrocarbons are stored in adsorbed state inside kerogen. Because of the organic nature of kerogen pores, as well as the large surface area, adsorbed hydrocarbons cannot be ignored when calculating original gas in place (Ambrose et al., 2012). For the purpose of forecasting shale gas production, Langmuir model has been adopted by the industry to estimate adsorbed gas amount, mostly because of its simplicity.

$$\frac{V_s}{V_{sL}} = \frac{P}{P_L+P} \tag{1}$$

The limitation of Langmuir model is that the theory assumes a fixed number of adsorption sites with have uniform properties are available on the surface, and each

adsorption site holds maximum of one gas molecule. Under the reservoir conditions, Langmuir isotherm may not represent the true multi-layer adsorption behavior of gas adsorption.

To compensate the limitation of mono layer adsorption, BET theory has been proposed to quantify the adsorbed gas amount at high pressure. It can be expressed as follows:

$$v(p) = \frac{v_m C p}{(p_0 - p)[1+(C-1)p/p_0]} \quad (2)$$

The difficulty in applying BET theory to shale reservoir is that it requires the knowledge of the fluid's saturation pressure ($p_0$). BET theory assumes the kinetics of adsorption and desorption is the same process as equilibrium between gas phase and liquid phase. This assumption may work reasonably under certain conditions but, for the typical condition of shale reservoirs, methane-rich natural gas is mostly in supercritical state where there is no clear distinction between the vapor and the liquid phases. Thus the idea of saturation pressure is not applicable.

Additionally, BET theory considers only the kinetic process between the fluid molecules and the surface. As pressure is increased, the theory assumes all the fluid molecules will be liquefied and thus considered as adsorbed phase. However, in shale gas reservoir, pressure increase may not induce phase change. Higher pressure will only lead to a denser fluid, where the fluid-fluid interaction may become compatible with the fluid-surface interaction. A detailed illustration of this case will be shown in the upcoming pages related to Monte Carlo (MC) simulation.

Another method to estimate gas adsorption is by molecular simulation. One of the commonly used methods in simulating equilibrium fluid-solid system is by Monte Carlo simulation. During the simulation, the total energy of the system is computed repetitively. According to Boltzmann probability theory, the probability of a state is proportional to its energy. Therefore, as simulation goes on, the algorithm will drive the system toward the most probable state, which is also the most energy stable state.

Monte Carlo simulations have been used for many purposes including prediction of bulk fluid property and fluid phase transition. In 1980s, Monte Carlo simulation was applied to study adsorption phenomenon in zeolites, another naturally-occurring nanoporous material (Soto and Myers, 1981; Woods and Rowlinson, 1989). These simulations have provided valuable insights into adsorption and demonstrated that the Monte Carlo simulation is a reliable tool in the study of adsorption.

To investigate natural gas adsorption behavior in organic-rich shale, Diaz-Campos and Akkutlu (2012), used Monte Carlo simulation technique. Their study has revealed methane density profile inside a nano-channel. Their result indicated mono-layer adsorption model (e.g., Langmuir isotherm) may not be sufficient when estimating gas in place under reservoir condition.

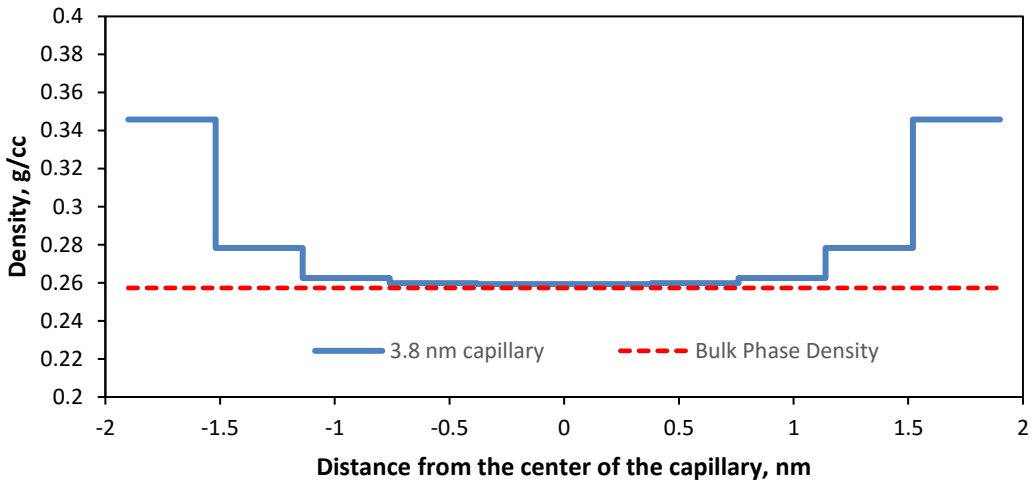


**Figure 1 — Density profile of methane at 176 °f (80 °c) in pore widths of 4nm**

Figure 1 shows that adsorption will cause heterogeneous density distribution on the radial direction of capillary under the reservoir conditions. It clearly shows multi-layer adsorption behavior of methane on the walls. Following the adsorption layer, which is the first molecular layer by the wall, there exist transition layers of molecules, where the density is higher than the bulk phase fluid at the central portion of the pore, but less than that of the adsorption layer molecules.

In Monte Carlo simulation section of this thesis, the same simulation set up used by Diaz-Campos and Akkutlu is considered. By varying the capillary size and pressure, density profile of methane is plotted inside single-wall carbon nanotube, CNT, to study the competitive process of fluid-fluid interaction as oppose to fluid-surface interaction at different pressure.

## 1.2 Viscous Flow

Unlike the general recognition of adsorption effect on gas in-place calculation, the effect of adsorption on transport is not sufficiently accounted. Therefore, the rest of Section 1 is dedicated to the transport phenomenon of a hydrocarbon fluids in tube. To begin with, we introduce the most commonly observed flow mechanism, the viscous flow.

Viscous flow in a capillary can be represented by Hagen-Poiseuille equation. To derive Hagen-Poiseuille equation, we can simply start from viscous force equation, where we assume that the fluid has homogeneous density and viscosity:

$$\mathrm{F}_{viscosity,\ \text{inner layer}} = -\mu A \frac{\Delta v_x}{\Delta y} \tag{3}$$

We consider the case of 1-D laminar flow in x-direction, where flow across the tube is considered by the molecular layers. Hence, the center layer in the tube has the largest velocity. When the flow system reaches steady-state, the combined forces from the pressure gradient and the two viscous forces from the neighboring layers must equal zero.

$$0 = \mathrm{F}_{pressure\ gradient} + \mathrm{F}_{viscous,\ \text{inner layer}} + \mathrm{F}_{viscus,\ \text{outer layer}} \tag{4}$$

$$0 = -\Delta P 2\pi r dr - \mu 2\pi r \Delta x \frac{dv_r}{dr} + \mu 2\pi (r + dr)\Delta x \frac{dv_{r+dr}}{dr} \tag{5}$$

Let us simplify the above equation using Taylor series expansion and ignoring the quadratic term of *dr*, we have

$$\frac{1}{\mu}\frac{\Delta P}{\Delta x} = \frac{d^2 v}{dr^2} + \frac{1}{r}\frac{dv}{dr} \tag{6}$$

Now, we apply the following boundary condition to solve for the flow velocity v(r):

(1) No-Slip boundary condition, with v(r) = 0 at r = R

(2) Axial symmetry, $\frac{dV}{dr} = 0 \; at \; r = 0$

We have the following formulation for velocity of liquid moving through the tube as a function of the distance from the center of the tube.

$$v(r) = -\frac{R^2}{4\mu}[1 - (\frac{r}{R})^2]\nabla P \tag{7}$$

where:

v = flow velocity, $m/s$

r = distance of the flow layer to capillary center, $m$

R = radius of the capillary, $m$

$\mu$ = viscosity, $Pa\ s$

$\nabla P$ = pressure gradient, $Pa/m$

By simply integrating equation (7) over the cross-sectional area perpendicular to flow, one can easily show the analogy of Hagen-Poiseuille flow in pipe to Darcy flow in porous media:

$$< v >= \frac{2}{R^2}\int_0^R v\, r dr = -\frac{R^2}{8\mu}\nabla P \tag{8}$$

One can recognize that, after integration over the flow area, HP flow equation has the same structure as Darcy's equation. In the case of cylindrical 1-D flow, permeability *k* of the tube simply equals to $R^2/8$.

Volume flux of HP flow then can also be formulated as follows:

$$Q = < v > \pi R^2 = -\frac{\pi R^4}{8\mu} \nabla P \tag{9}$$

Mass flux of convective transport, as described by the HP flow equation or Darcy's law, is proportional to pressure gradient as well as flow area. Velocity profile of convection is characterized by a parabolic shape. At the center of the capillary, where the least resistance exists, the fluid flow velocity has its maximum value, whereas, at the boundaries, the velocity is reduced to zero.

For a certain fluid under constant pressure gradient, mass flux of flow is proportional to the capillary radius by a power of 4, which ties mass flux directly to the capillary size. This character of fluid flow brings out the conventionally accepted belief that permeability is an intrinsic property of the tube or the porous medium. In later section, we will show that this belief is true only if convection is the dominant transport regime.

## 1.3 Viscosity Based On Kinetic Theory Of Gas

With the knowledge that viscous force is essential for convection, we can now focus to kinetic theory of gases to compute viscosity. To begin with, we need to lay out several assumptions of classical mechanics in kinetic theory:

First, kinetic theory of gases is based on classical mechanics but not quantum mechanics. This means kinetic theory of gases follows Newton's equations of motion. Secondly, kinetic theory of gases assumes a gas in the Maxwellian state, where

molecules are point centered molecules with force repelling each other inversely proportional to the fifth power of their distance. Maxwellian state also requires the gradients of flow are sufficiently small so that the gas can be considered in local equilibrium.

Consider a dilute gas system with *n* number of molecules per unit volume. Let symbol $\Psi$ denote property of a single molecule that can be changed by collisions. Then, $< \Psi >$ represents the average value of $\Psi$ for the dilute gas system. Based on the concept of mean free path $l$, we can set up the following model.

As shown in Figure 2, molecule from the left travels a distance equal to mean free path then collide with molecule from the right. Molecules crossing the plane z from z-$l$ side will transfer property$\Psi_{z-l}$, and those crossing from z+$l$ side will transfer property$\Psi_{z+l}$.

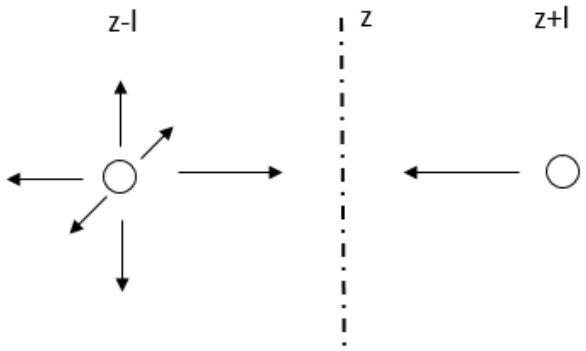


**Figure 2 — Illustration of molecules transferring property during collision.**

The net molecular flux of the property Ψ in the direction z can be calculated by

$$F_{\Psi,z} = \Gamma_{z-l} < \Psi_{z-l} > -\Gamma_{z+l} < \Psi_{z+l} > \quad (10)$$

where $\Gamma_{z-l}$ denotes number of molecules per unit area per second crossing the plane z. Because only 1/6 of molecules on plane $\Gamma_{z-l}$ move in the direction of (+z),

$$\Gamma_{z-l} = \Gamma_{z+l} = \frac{1}{6} < C > * n \quad (11)$$

Here, $< C >$ is the mean value of the thermal speed. Next, substitute the equality $\Gamma_{z-l} = \Gamma_{z-l}$ into Eq (10). Then we have

$$F_{\Psi,z} = \Gamma_{z-l} < \Psi_{z-l} > -\Gamma_{z+l} < \Psi_{z+l} > \quad (12)$$

$$= \frac{1}{6} < C > * n * (< \Psi_{z-l} > - < \Psi_{z+l} >$$

$$= \frac{2l * < C >}{6} n \frac{(< \Psi_{z-l} > - < \Psi_{z+l} >}{2l} \approx - \frac{l * < C >}{3} n \frac{d < \Psi >}{dz}$$

Now, we can bring in different property into F function and link the macro scale bulk property with micro scale particle movement. When we substitute Ψ with momentum per molecule, $mv_y$, we can calculate the bulk viscosity as follows

$$F_{mv_y z} = - \frac{< C >}{3} * l * n * m \frac{d < v_y >}{dz} = -\mu \frac{d < v_y >}{dz} \quad (13)$$

$$\mu = \frac{< C >}{3} * l * n * m \quad (14)$$

As shown above, calculation of macroscopic property of viscosity have been related to the microscopic property of mean free path and molecular velocity. The mean value of molecular velocity and mean free path for a gas in absolute Maxwellian state can be estimated as:

$$< C >= 2\sqrt{\frac{2kT}{\pi m}} \tag{15}$$

$$l = \frac{1}{\sqrt{2}\pi d^2 * n} \tag{16}$$

Therefore, viscosity can be calculated as:

$$\mu = \frac{<C>}{3} * l * n * m = \frac{2}{3d\pi^2}\sqrt{\frac{kmT}{\pi}} \tag{17}$$

Other than using estimated values based on Maxwellian assumptions, another way of calculating the mean free path and molecular velocity is to perform molecular dynamics simulation. In nonequilibrium simulation section of this thesis, we build a molecular simulation model to track mean free path of molecules and predict viscosity assuming the fluid can be considered as a dilute gas. By averaging mean free path values of a group of molecules over simulation, we calculated supercritical methane viscosity in nano-capillary.

## 1.4 Diffusion

Other than viscos flow, diffusion is another transport mechanism that can contribute to total mass flux of fluid flowing in a tube. There are mainly two types of diffusions, self-diffusion and mutual diffusion. It is important to distinguish these two types of diffusion before using them in the estimation of mass flux.

Self-diffusion occurs in the absence of any concentration (or chemical potential) gradient. It describes the transport of molecules caused by intermolecular collisions, i.e., Brownian motion. Because self-diffusion occurs in a single-component equilibrium

system, the result of self-diffusion is simply the fluid molecules changing positions within the system.

On the other hand, mutual diffusion occurs in the presence of a concentration (or chemical potential) gradient. It is the non-equilibrium process that results in net transport of mass. Therefore, mutual diffusion is also called chemical diffusion or transport diffusion. Mutual diffusion is the transport mechanism often associated with the release of substance from matrices into solutions. For example, in medical research domain, the process of drug release from a hydrogel matrix is mainly associated with mutual diffusion (Gagnon and Lafleur, 2009). This process is identical to the process of natural gas release from shale, therefore in the following parts of thesis we ignore self-diffusion and focus on mutual diffusion.

Mutual diffusion phenomena is often described using Fick's law. In the case of single component gas, diffusion flux is proportional to concentration gradient:

$$J = -D\frac{\partial C}{\partial x} \tag{18}$$

where:

J = diffusion flux, $\frac{mol}{m^2 s}$

D = diffusion coefficient or diffusivity, $\frac{m^2}{s}$

C = molar density of gas per unit volume, $\frac{mol}{m^2 s}$

$x$ = location, $m$

To calculate the mass flux caused by mutual diffusion in a capillary, we need only multiply the diffusion flux by the product of flow area A and molecular weight M:

$$q = J * A * M = -\pi R^2 DM \frac{\partial C}{\partial x} \quad (19)$$

Equation (19) shows one of the reasons why mass flux contribution of diffusion is usually omitted in conventional petroleum reservoir simulation. In the case of diffusion, mass flux increase with the increase of capillary size by power of 2, whereas in convection, mass flux increase with capillary size by power of 4. Hence, as pore size increases, convective mass flux increases much faster, making convection the dominate transport mechanism. However, when we consider natural gas flow in tight shale matrices, where the size of capillary is extremely small, under certain conditions, diffusional flux may make a substantial contribution to the total mass flux, therefore it should not be omitted.

In fact, combining diffusion and convection in fluid transport is not new to the petroleum industry. When simulating tracer injection or chemical flooding during an enhanced oil recovery operation, a convective-diffusive equation is used to model the transport of the injected chemical. Even though convection is still the dominating flow regime during the injection operation, we are interested in the accurate location and concentration of the injected chemical. Therefore, diffusion flux needs to be integrated into the flow equation. A general structure of convection-diffusion equation is

$$\nabla \cdot (D \nabla c) - \nabla \cdot (\vec{v} c) + R = \frac{\partial c}{\partial t} \quad (20)$$

c = concentration of substance of interest, $\frac{mol}{m^3}$

D = tortuosity-corrected diffusion coefficient or diffusivity, $\frac{m^2}{s}$

R = source or sink, $\frac{mol}{m^3 s}$

$t$ = time, $s$

$\vec{v}$ = velocity of substance moving caused by convection, $m/s$

Another example application of convective-diffusive transport equation is Klinkenberg's slip correction for gas flow in capillaries. In reservoir engineering applications, Klinkenberg's slip correction is used to quantify the gas flow contribution of slipping molecules by the capillary walls at low pressures. One can show Klinkenberg's slip correction along with the convection-diffusion equation and utilizing Knudsen diffusion coefficient. Detailed derivation are shown below.

Total molar flux $J$ due to convection and diffusion:

$$J = -(\frac{k}{\mu}p + D_k)\frac{1}{RT}\frac{\partial p}{\partial x} \tag{21}$$

To convert the molar flux $J$ to volume flux $q$, we have

$$J = \frac{p}{RT}q \tag{22}$$

Combining the two equations above, we have

$$\frac{p}{RT}q = -(\frac{k}{\mu}p + D_k)\frac{1}{RT}\frac{\partial p}{\partial x} \tag{23}$$

$$q = -\frac{k}{\mu}(1 + \frac{D_k\mu}{k}\frac{1}{p})\frac{\partial p}{\partial x} \tag{24}$$

Now, we replace $\frac{D_k\mu}{k} = b$, and obtain convection-diffusion equation as follows:

$$q = -\frac{k}{\mu}(1 + \frac{b}{p})\frac{\partial p}{\partial x} \quad (25)$$

This is the same form as given by Klinkenberg (1941) where he hs introduced an apparent gas permeability as follows:

$$k_g = k(1 + \frac{b}{p}) \quad (26)$$

where:

$k_g$ = apparent permeability calculated from gas flow tests;

$k$ =absolute permeability of the rock;

p =flowing pressure of the gas in the system;

b =Klinkenberg factor, a constant for a particular gas in a porous medium.

The well-known Klinkenberg's equation for gas slippage correction is in fact a simple but consistent form of the convection-diffusion equation. This implicitly demonstrates the necessity under certain conditions, to incorporate into total mass flux. When diffusion flux cannot be neglected, it contributes and enhance mass flux in a homogeneous way, which means an increase of velocity at all locations.

## 1.5 Surface Diffusion

Surface diffusion is a transport mechanism associated with the adsorption phenomenon. It is most commonly explained by hopping mechanism, defined as

adsorbed molecules transport to nearby adsorption sites. Illustration of hopping mechanism and adsorption-desorption is shown in Figure 3.

To initiate the hopping movement, a molecule has to overcome an activation energy. The activation energy needs to be smaller than the desorption energy, otherwise desorption process would be dominant. Diffusion coefficient of hopping mechanism can be calculated using Arrhenius equation including activation energy. However, molecules transport along the surface is a complex process which may involve multiple mechanisms than just hopping. Two categories of surface diffusion has been identified: adatom diffusion and cluster diffusion. Adatom diffusion describe the movement of an atom moving from one adsorption site to another. Mechanisms of adatom diffusion includes hopping, atomic exchange and vacancy diffusion. Cluster diffusion describes motion of a group of adsorbed molecules moving along the surface. Mechanisms of cluster diffusion includes dislocation, glide diffusion and shearing.

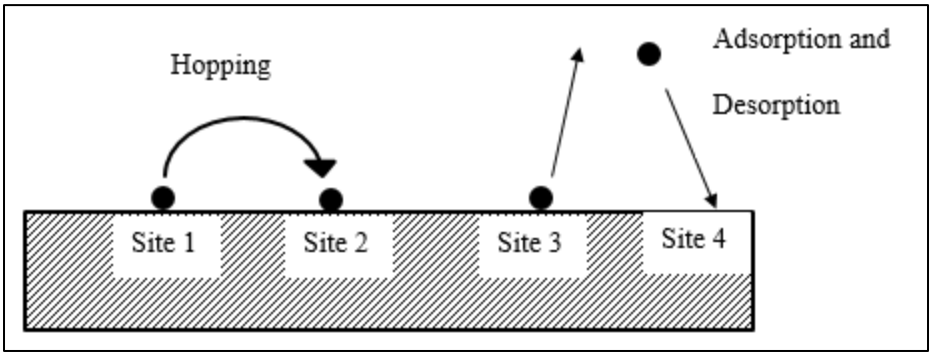


**Figure 3 — Illustration of hopping mechanism versus adsorption and desorption.**

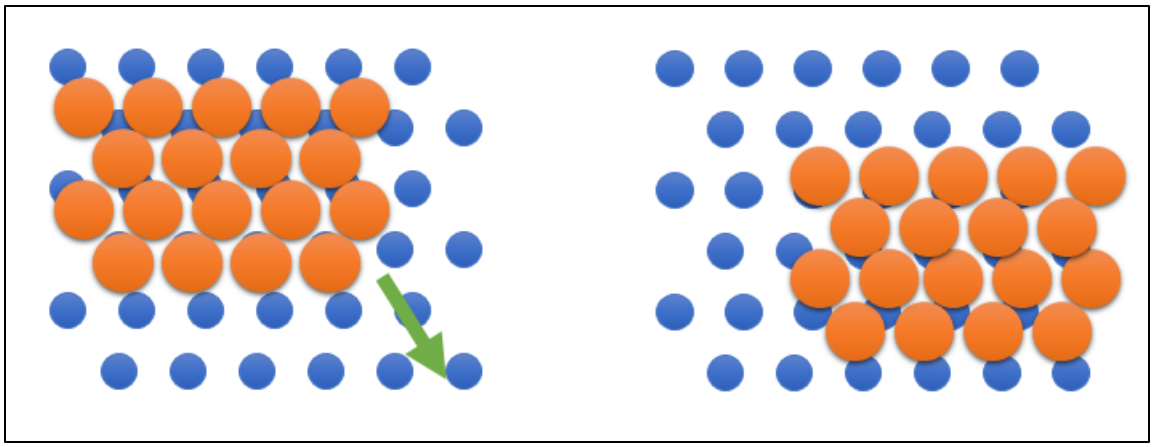

**Figure 4 — Illustration of gliding mechanism of cluster diffusion.**

Cluster diffusion is important in many non-equilibrium growth process in physics, chemistry and biology. A number of investigations have been dedicated to the microscopic characterization of the migration of small clusters on surface by field ion microscopy (FIM) (Kellog, G.L. 1994) and scanning tunneling microscopy (STM) (Michely et al., 1993). Imaging techniques provide initial and final position of the cluster, where the pathway can't be observed. For this purpose, MD simulation has been utilized to investigate mechanism of cluster diffusion. MD simulation results of this work show that, once a free molecule of methane is adsorbed onto the surface, it can be transported along the surface together with the other adsorbed molecules until its desorption occurs. Hence, the adsorbed molecules of methane experience cluster diffusion. We also observe that the adsorbed-phase velocity is a function of pressure gradient. This allows us to quantify this phenomenon into an adsorbed phase mobility coefficient, which can be used to calculate the adsorbed phase velocity.

# 2. MOLECULAR SIMULATION SET UP

## 2.1 Equilibrium Monte Carlo Simulation

Before we study the transport of gas through nano-size capillary, it is important to understand gas adsorption phenomenon inside the capillary under equilibrium. One of the methods used is NPT Monte-Carlo simulation.

The equilibrium Monte-Carlo simulation system consists two simulation boxes. One simulation box contains bulk phase methane molecules with periodic boundary conditions. Number of molecules (N), pressure (P) and temperature (T) of this simulation box were fixed throughout the simulation. Volume is the changing parameter of this simulation box. The other box simulate slitshape organic nano capillary by two parallel graphite walls. The interaction between the wall and the fluid molecules are calculated using the Steele Wall potential, which is a 10-4 Lennard –Jones potential.

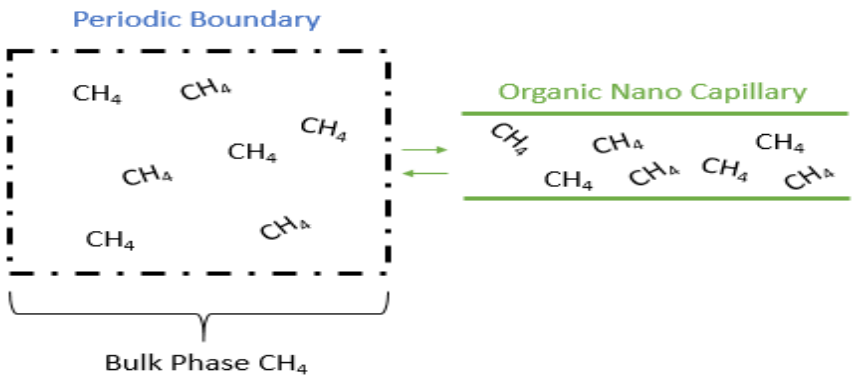


**Figure 5 — Two-box Monte Carlo equilibrium simulation system**

| Table 1 Lennard-Jones Parameters for Methane and Steele Wall | | |
|---|---|---|
| Atom/molecule | $\sigma, nm$ | $\varepsilon/K_B, K$ |
| Methane | 0.373 | 148.0 |
| Steele Wall | 0.34 | 28.0 |

Methane is modeled as united atoms by TraPPE-UA force field. Interaction between methane molecules are calculated by 12-6 Lennard-Jones potential. Lennard-Jones parameters of methane and Steele Wall are listed in Table 1.

During simulation, methane molecules move freely between two simulation boxes to achieve thermal dynamic equilibrium condition. We run the simulation for at least $3\times10^5$ cycles to make sure system reaches equilibrium. Then we analyze output coordinates file (.pdb file) which contains methane molecules locations, to calculate methane density profile between capillary walls.

We repeated the Monte Carlo simulations with different capillaries of changing sizes (1.52nm, 2.28nm and 3.8 nm) and at different fluid pressure values (3000psia, 5000psia and 9000psia). This allows us to study how adsorption behavior changes due to variations in capillary size and pressure. Detailed result will be shown in Section 3. Simulation Results and Discussions.

## 2.2 Nonequilibrium Molecular Dynamics Simulation

Molecular dynamics in general is a simulation method to study movement of atoms and molecules in time. During each time step of the simulation, interaction force between molecules and atoms are calculated based on Lennard-Jones potential (6-12 potential). At the next simulation time step, locations and velocity of molecules and atoms are updated by combining previous time step location, previous time step velocity and previous time step force. In our simulation, because of the symmetrical tetrahedral structure of methane molecules, we used united atom force field (OPLS-UA) which treat methane molecules as a united atom.

To build a piston like simulation system, we need to construct three fundamental structures: piston, source/sink tank and a carbon nano tube connecting source/ sink tanks. As shown in Figure 6, the vertical graphene sheet shown in red on the left represents the piston. The other two blue graphene walls in the middle represent walls of source/sink tank, and hollowed CNT in between the walls represents the organic capillary.

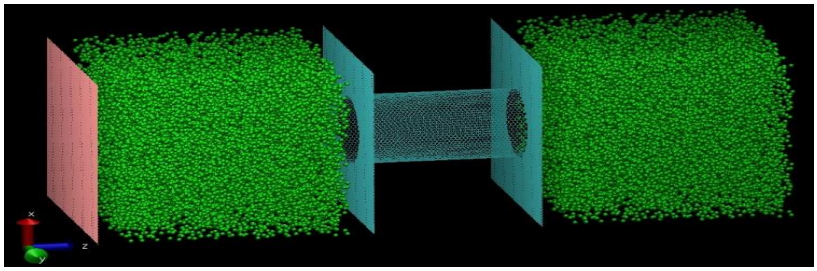

**Figure 6 — Steady state flow system 6nm diameter**

This model was previously developed in our group and the detailed simulation methodology can be found in Riewchotisakul and Akkutlu (2015). A similar model was developed by Thomas and McGaughey (2009) to analyze water flow in carbon tube. At the beginning of the simulation a certain amount of methane molecules are charged into the source and sink tanks and let the simulation run without moving the piston for about 1,000picoseconds. Pressure drops initially due to methane molecules adsorbing to the graphene walls and piston. After the initial pressure drop, which is caused by methane molecules fill up the empty space in carbon nanotube, the fluid pressure in the tanks decreases slowly until a stable pressure is reached, shown in Figure 7.

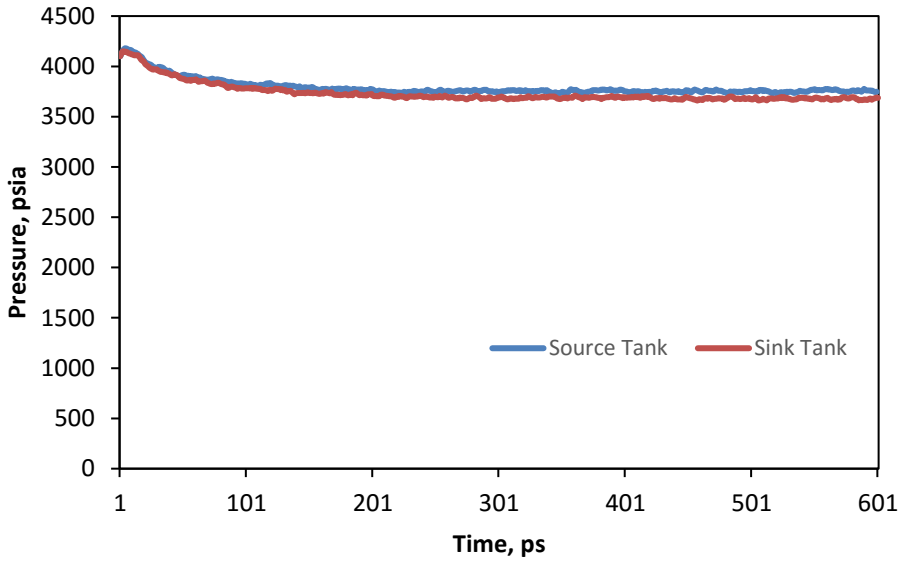


**Figure 7 — Equalization of the source and sink tank fluid pressure**

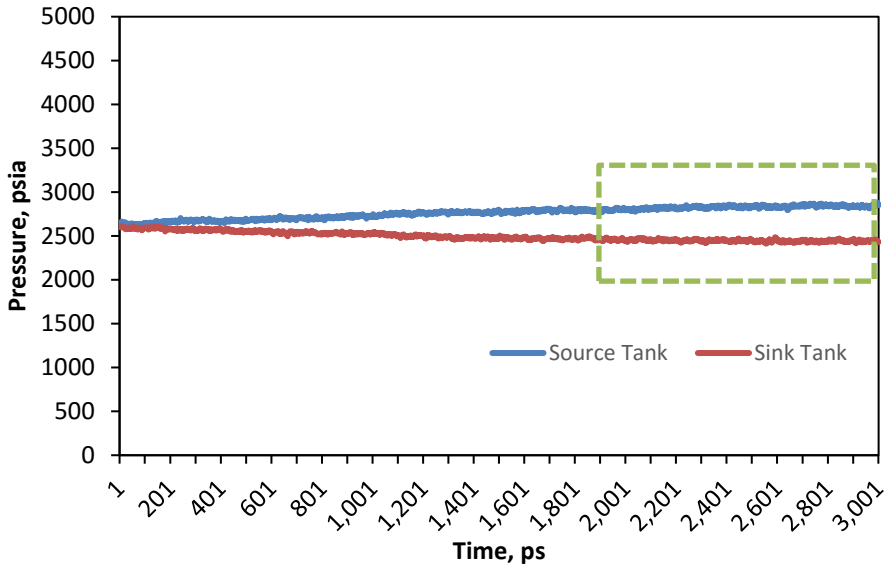


**Figure 8 — Steady-state flow period identified by the stabilized fluid pressure values within the green-dotted rectangle**

Once pressure equalized in the system, we start pushing piston to create differential pressure between sources and sink tank. The simulation stops when the piston reaches to the other wall of the upstream tank. As shown in the plot below, once the piston starts moving, the source tank volume will decrease and the sink tank volume will accordingly increase due to periodical boundary conditions at the outermost ends. At the same time, the differential fluid pressure between the tanks will initiate flow from the source tank to the sink tank through the carbon nanotube. At one point, the flow of methane molecules are able to counter balance volume change of the tanks, creating a steady-state flow condition.

Figure 8 shows typical pressure response under steady-state. The steady-state period of flow chosen for quantitative analysis of transport is marked by green rectangle. With the steady-state flow period identified, we extract location and velocity information of all the methane molecules during their steady-state flow through carbon nanotube. Using an in-house Python code "Location.py" and "Velocity.py", density profile is generated by counting number of molecules per unit volume, velocity profile is generated by average velocity values on the Z direction (axial direction of CNT) for all steady-state frames. Detailed results will be shown in Section 3.

## 2.3 Mean Free Path Simulation Set Up

Based on kinetic gas theory in Section 1.3, we can calculate methane viscosity using mean free path and thermal speed of molecules.

$$\mu = \frac{<c>}{3} * l * n * m \tag{27}$$

where

$\mu$ = viscosity, pa.s

$< C >$ = thermal speed, m/s

$l$ = mean free path, m

n =number of molecules per unit volume, molecules/$m^3$

m =mass of methane molecule, kg/molecule

Here to calculate thermal speed and mean free path, we set up our viscosity simulation based on the previously explained piston model. First we run the piston model without

moving the piston to make sure system achieve equilibrium. Then we remove both source tank and sink tank and adjust simulation box size so that it contains only CNT filled with methane molecules. Lastly, we run MD simulation with the new model for 1,000 femtosecond and record location and velocity of all molecules every 2 fs, which ensures all collisions are captured (Prabha et al., 2013) for the analysis.

Thermal speed <C> is the averaged instantaneous speed of all molecules in the simulation system. For each molecule, the instantaneous speed is calculated as

$$C = \sqrt[2]{{v_x}^2 + {v_y}^2 + {v_z}^2} \tag{28}$$

Then <C> is calculated by first averaging all molecules' instantaneous speeds over all simulation time steps.

Mean free path is defined as molecule's travel distance between two successive collisions. It can be calculated as

$$l = < t_{free} > \times < C > \tag{29}$$

where

$l$ = mean free path, m

$< t_{free} >$ = averaged free travel time, s

$< C >$ = thermal speed, m/s

To calculate the averaged free travel time, we track collision status of target molecules by calculating their intermolecular distance. At each time step, we calculate the inter-molecular distance between our target molecule and all other molecules. If the

intermolecular distance is less than $\sigma$, we register the target molecule as within "collision", otherwise we register the target molecule as "free". We record the length of free time, which represents the time that a molecule travels in space without colliding with any other molecules. By repeating this process on different molecules, we can calculate average free time of the molecules. Mean free path of molecules can be calculated by multiplying average free time by thermal speed of molecules. Detailed simulation result of average free time, thermal speed and viscosity will be shown in Section 3.

# 3. SIMULATION RESULTS AND DISCUSSIONS

## 3.1 Monte Carlo Simulation Results

Figure 9 shows methane density across the diameter of the capillary by discrete band for every 0.38 nm, which is equal to the kinetic diameter of a methane molecule. Here we show density profile of methane in three different capillaries with diameter, 3.8nm, 2.28nm, and 1.52nm. In the case of 3.8 nm capillary, we can clearly observe multi-layer adsorption, characterized by a denser adsorption layer by the CNT wall, followed by three transition layers, and free methane fluid in the middle of capillary with density equal to bulk phase methane density. Here we define free fluid as methane molecules free from the influences of the walls.

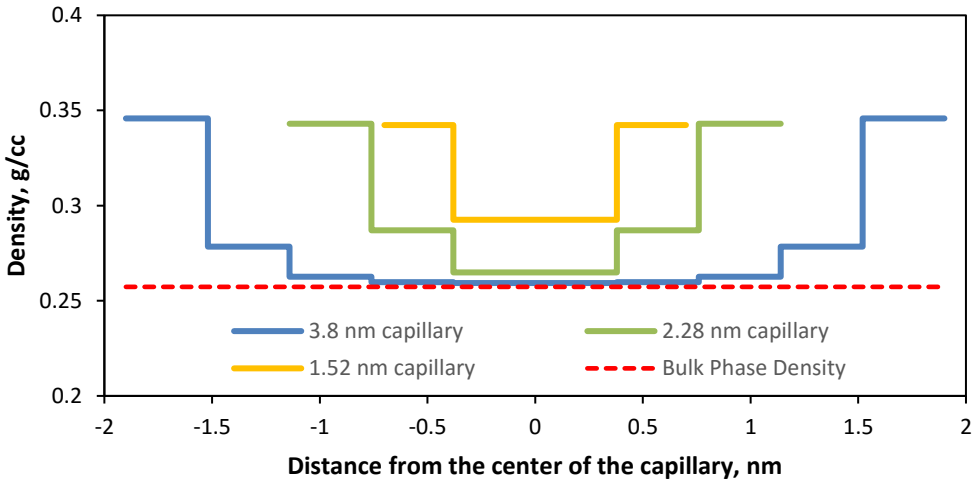


**Figure 9 — Density profile for methane within different sizes of capillary at pressure of 9,000psia, temperature of 175 °F (353 °K)**

Compared to the commonly used storage model, the Monte Carlo simulations show extra amount of gas associated with the transition layers exist. For example at the center the density goes up from 0.26g/cc to 0.29 g/cc at the center. We suggest this extra amount of fluid should be counted as excess gas during the storage calculations.

In the case of 1.52 nm capillary the pore space is only capable of containing 4 layers of adsorbed methane molecules. Transition layer of methane from each side of the boundary have reached into and occupied the center of capillary, which makes methane density at the center of capillary higher than the other two cases (Figure 9). This observation is important because it also sheds light on possible transport regime of small capillaries with 2nm size or less. With all pore space occupied by the adsorbed phase fluid, the dominating transport regime for these capillaries will necessarily be the surface transport.

We also conduct the simulation at 3,000psi and 5,000psi. To compare the density profile at different pressure, we introduce “density ratio” defined as simulation density at each layer divided by bulk phase density. As shown below, at low pressure (3000psi) adsorbed phase density is 2.5 times of bulk phase density. At medium pressure (5000psi), adsorbed phase density is between 1.5 to 2 times of the bulk phase density. At high pressure (9000psi), adsorbed phase density is less than 1.5 times of bulk phase density

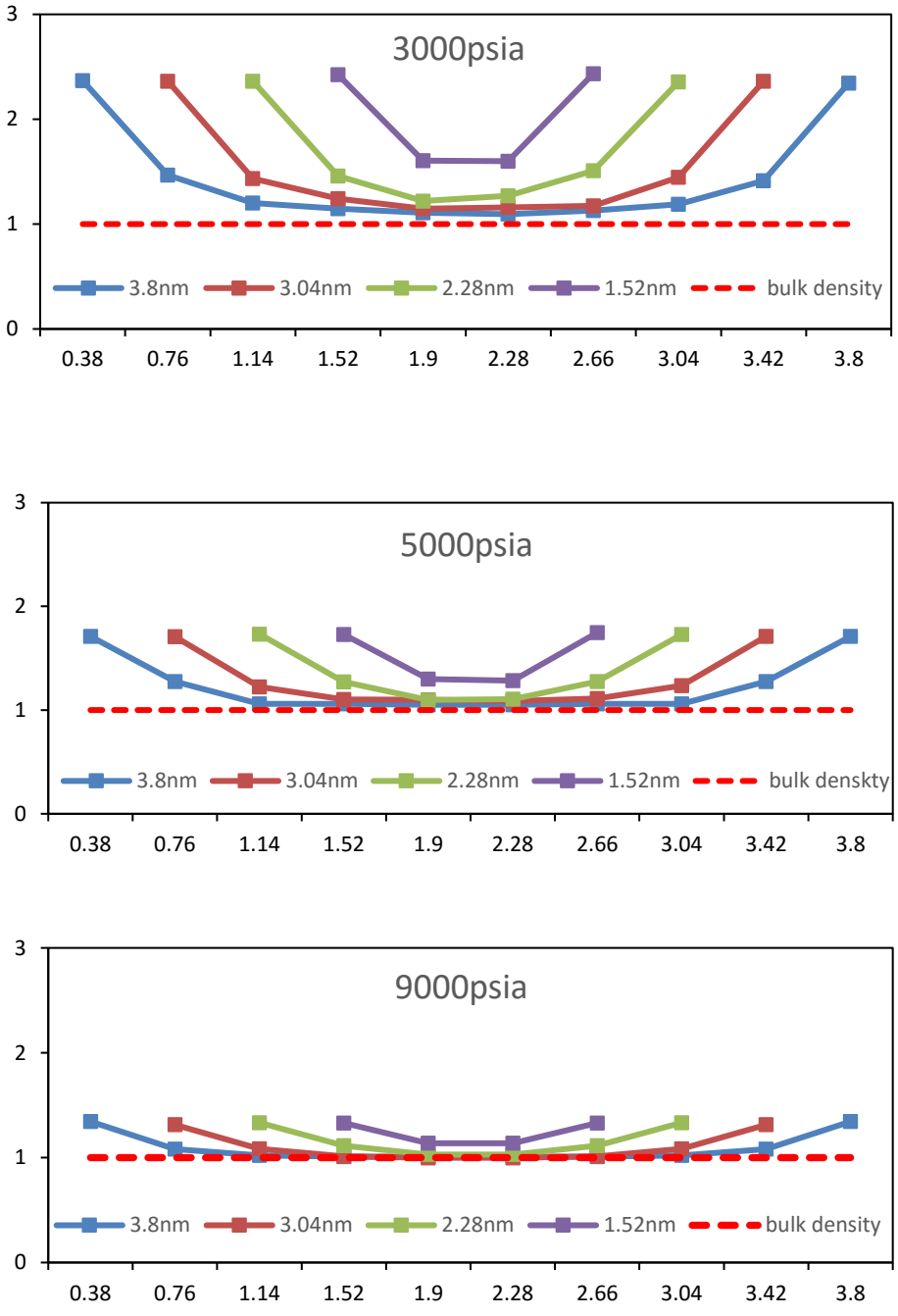


**Figure 10 — Comparison for methane density inside kerogen pores at various pressure: Top: 3000psia, Middle: 5000psia, and Bottom: 9000psia.**

We explain this phenomenon as a result of two competing processes: the fluid-fluid molecular interaction versus the fluid-wall interactions. Methane has critical pressure of 667psi and critical temperature of 190K. At typical reservoir pressure and temperature conditions, methane is in supercritical region of its phase diagram. In this region of the diagram, with pressure increase, methane behaves more like liquid and less like gas. At low pressure, strong Van der Waals interaction between fluid and surface lead to significant amount of adsorbed phase. At high pressure the number of molecules per unit pore volume is increased. This compression effect leads to a higher level of fluid-fluid interactions compared to the fluid-solid interactions experienced in the capillary. Van der Waals interaction between fluid molecules becomes stronger and even comparable to the fluid-surface interaction, leading to a less significant amount of adsorbed phase.

Monte-Carlo simulation results provide important insight into the pore space of nano-scale organic capillaries. The density heterogeneity requires engineers to treat the adsorbed phase and the free phase separately when estimating gas in place as well as and predicting fluid transport. In the next section, we present our results from Molecular Dynamic simulations. By simulating methane gas flow through carbon nanotube under steady-state flow condition, we aim to characterize different transport regimes and quantify the adsorbed phase transport mobility.

3.2 Density Profile Of Methane In Nanotube

As shown in the Monte Carlo simulation section (Figure 12 bottom), gas density in the organic nano-capillary is characterized by a high-density adsorption layer and several transition layers. In Figure 11 the density profile of methane during its steady-state flow through 6nm diameter nano-capillary is shown.

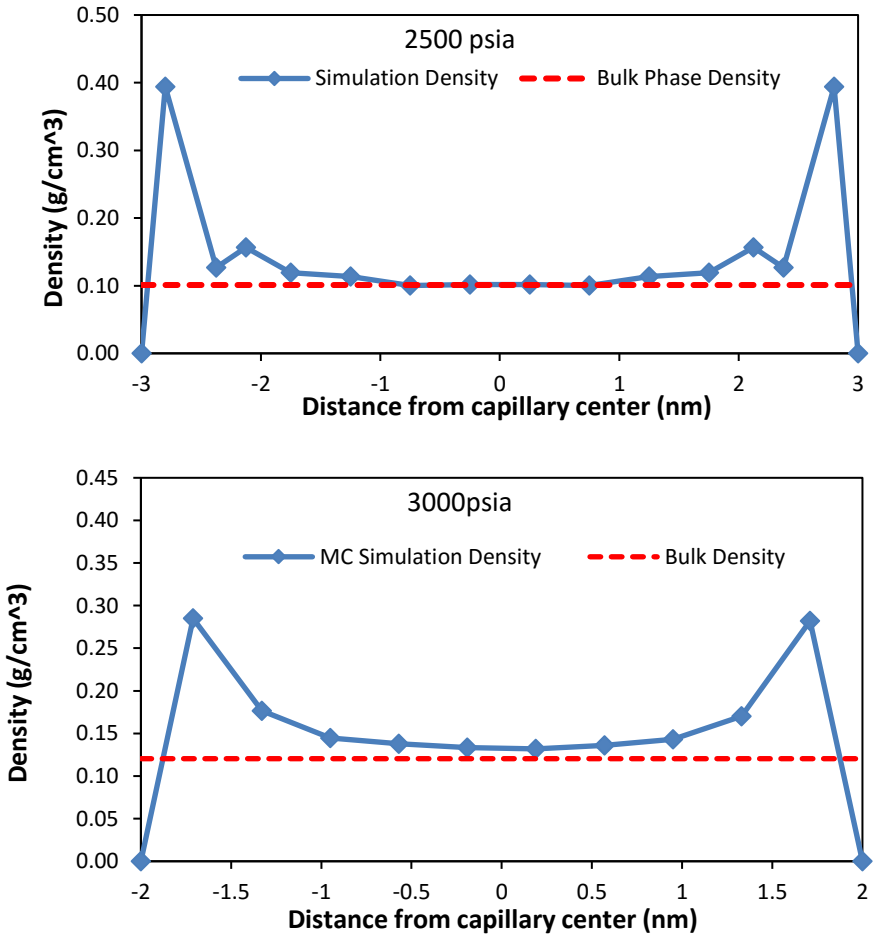


**Figure 11 — Density profile of methane in 6nm nanotube using MD simulation (top) Density of methane in 4nm slip shape pore using MC simulation (bottom)**

The plots show when methane flow through nanotube, there exists a density profile which is similar to that observed during the equilibrium simulation, which consists of one adsorption layer with several transition layers by the wall and bulk phase fluid in the middle. Even though the exact adsorbed layer density value does not match each other perfectly, it is due the different simulation methodology and different force field (Lennard Jones 12-6 vs Lennard Jones 12-4). This similar trend is important to us because it shows density heterogeneity of fluid inside organic capillary during viscous flow. In conventional transport theory, fluid density is considered to be homogeneous. Even though adsorption may happen, it is usually ignored due to the large size of capillary and overwhelming amount of bulk fluid participating in flow. Therefore in conventional theory, there is no need to differentiate adsorption phase fluid with bulk phase. However in the case of transport in nanotubes, size of capillary is at nanometer level, adsorption layers of molecules may change the total mass flux significantly (we will show detailed discussion in mass flux section). Therefore, it is necessary to differentiate adsorption phase with bulk phase and consider their transport separately.

## 3.3 Velocity Profile Of Methane In Nanotube

Next, we analyze velocity profile of methane molecules inside the nano-capillary. In our simulation, methane molecules flowing through carbon nanotube can be considered as 1-D flow in the main direction of the applied pressure gradient. Therefore, we analyze velocity vectors along the z-direction, which is the axial direction of the

tube. By averaging velocity of methane molecules inside the tube throughout the steady-state flow window, we plot velocity profile across the diameter of capillary as shown in Figure 11. Predicted velocity profile (in blue) is shown together with the classical (HP) viscous flow velocity profile (in dotted red) of the same pressure gradient and capillary size. In addition, density profile is plotted in the background (blue bar) to distinguish the free phase fluid from the adsorbed-phase fluid.

Figure 12 (Top) is methane velocity profile at large pressure gradient (60psi/nm). It shows the parabolic feature predicted by the HP equation. The strong parabolic shape in the simulation data indicates viscous flow is the dominant regime under the imposed flow condition. Consider now the velocity profile in Figure 12 (Middle), at a lower pressure gradient of 45 psi/nm, the parabolic shape of viscous flow still apparent but now relatively less significant. In Figure 12 (Bottom), when pressure gradient is decreased to 25 psi/nm, we notice that the velocity profile is almost lost. Instead of showing a maximum velocity at the center of capillary, the velocity profile is now uniform across the diameter of capillary and the velocity values show some degree of randomness. As mentioned in the introduction section of this paper, the uniform velocity profile indicates molecular diffusion. Hence, the observed gradual change in velocity profile in Figure 12 shows that viscous flow diminishes and pore diffusion becomes more pronounced with the further decrease of the pressure gradient. This transition can be better seen in Figure 13, where the three velocity profiles are plotted together.

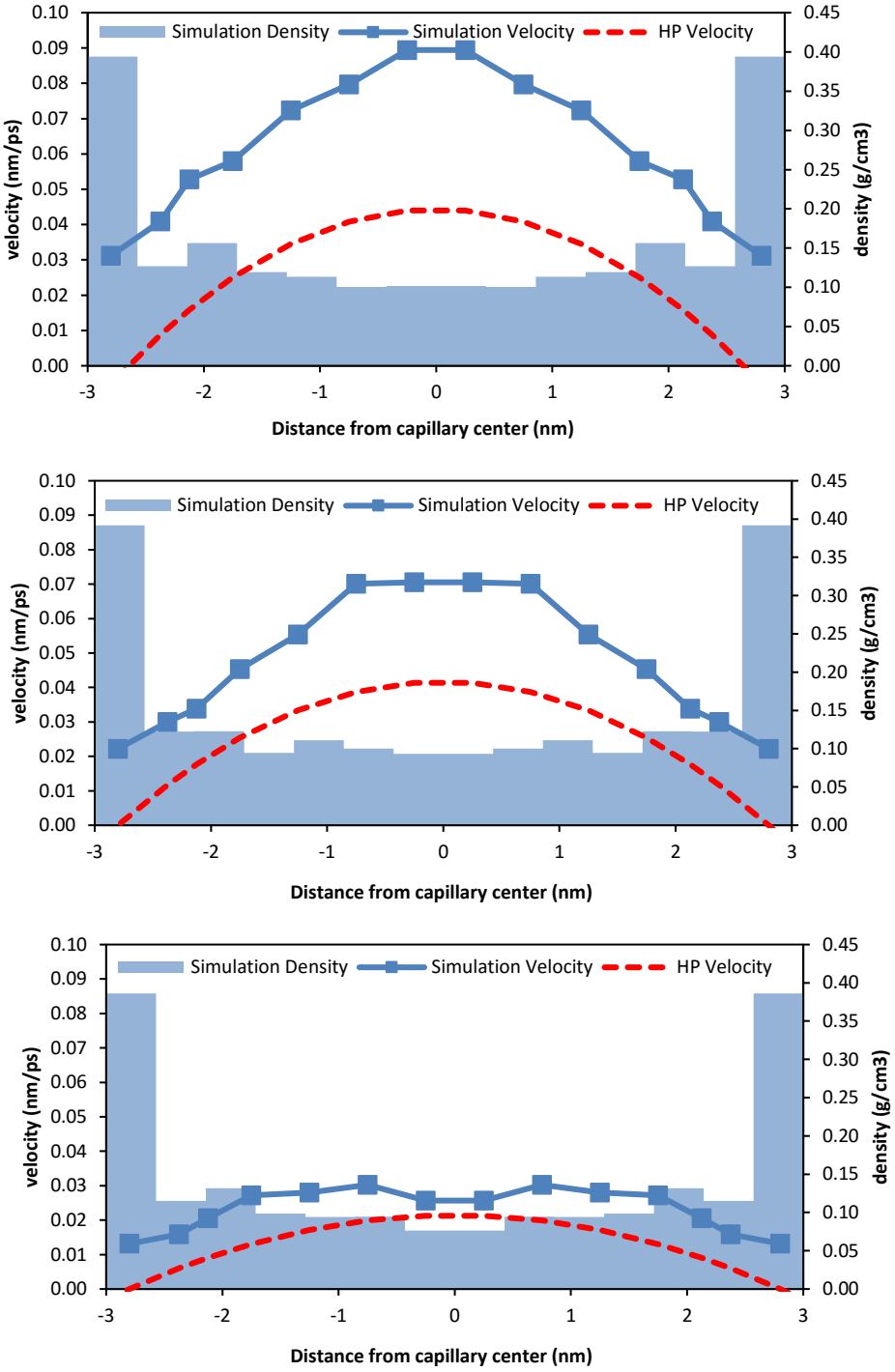


**Figure 12 — Methane velocity profile during steady-state flow at average pressure of 2500psia, temperature of 175 °F (353K). Pressure gradient is: Top: 60psi/nm, Middle: 45psi/nm, and Bottom: 25psi/nm**

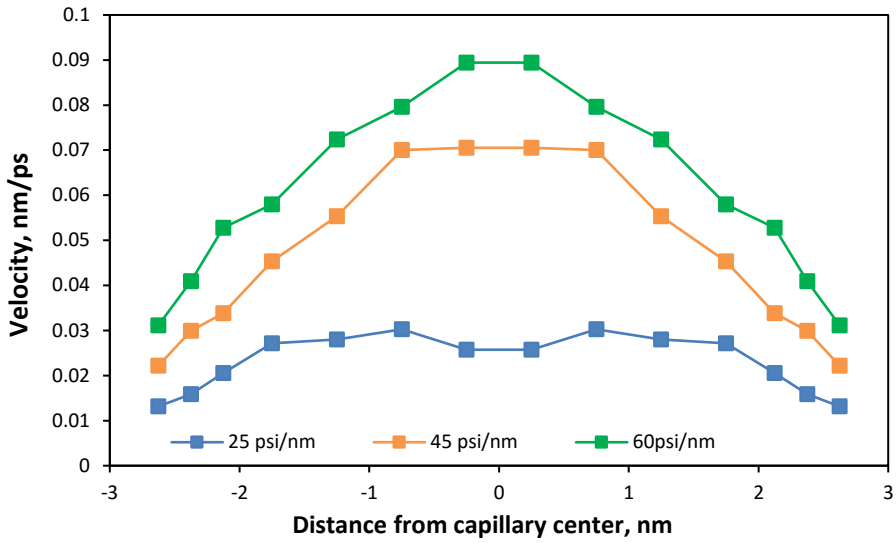


**Figure 13 — Methane velocity profile during steady-state flow under varying pressure gradient at average pressure of 2,500 Pisa, temperature of 175 °F (353 K)**

In all the three simulation cases considered, the simulation velocity profiles are consistently larger than the HP velocity, indicating that viscous flow is not the only mechanism contributing to total mass flux within the capillary. Here, because the simulation velocity profile has become uniform across the pore diameter at lower pressure gradient values, one would suggest that diffusion comes in and becomes another important mechanism contributing to the total mass transport. Hence, one would write:

$$v_{total} = v_{vis} + v_{diff} \tag{30}$$

We use HP velocity equation to estimate convection velocity contribution

$$v_{vis} = \frac{1}{4\mu}(r_{tube}^2 - r^2)\frac{\partial P}{\partial z} \tag{31}$$

Then, one can write the diffusion velocity equation and simplify it using the real gas law as follows:

$$J_{diff} = \rho v_{diff} = M_{CH4} D_K \frac{\partial C}{\partial x} \tag{32}$$

$$v_{diff} = \frac{M_{CH4}}{\rho} D_K \frac{\partial C}{\partial x} = \frac{1}{P} D_K \frac{\partial P}{\partial x} \tag{33}$$

$$v_{total} = [\frac{1}{4\mu}(r_{tube}^2 - r^2) + \frac{1}{P} D_K] \frac{\partial P}{\partial x} \tag{34}$$

Now, Using Equation 34, we plot $v_{total}$ as the dashed line (convection-diffusion line) and compare it with the simulation velocity in Figure 14. It shows velocity predicted by the analytical equation matches with the simulation result. Figure14 confirms the assumption that, at nano-scale total mass transfer inside the nano-capillary is a combination of convection and diffusion.

Contribution of diffusion is usually ignored at large scale natural gas transport problems because of the presence of an overwhelming amount of convective mass flux; however in the case of transport in nano-capillaries, diffusion contribution could be comparable to convection depending on capillary size and pressure effects. Because the capillary size of our problem is not infinitely larger than the mean free path of the methane molecules, we refer to mode of the observed diffusion as Knudsen diffusion.

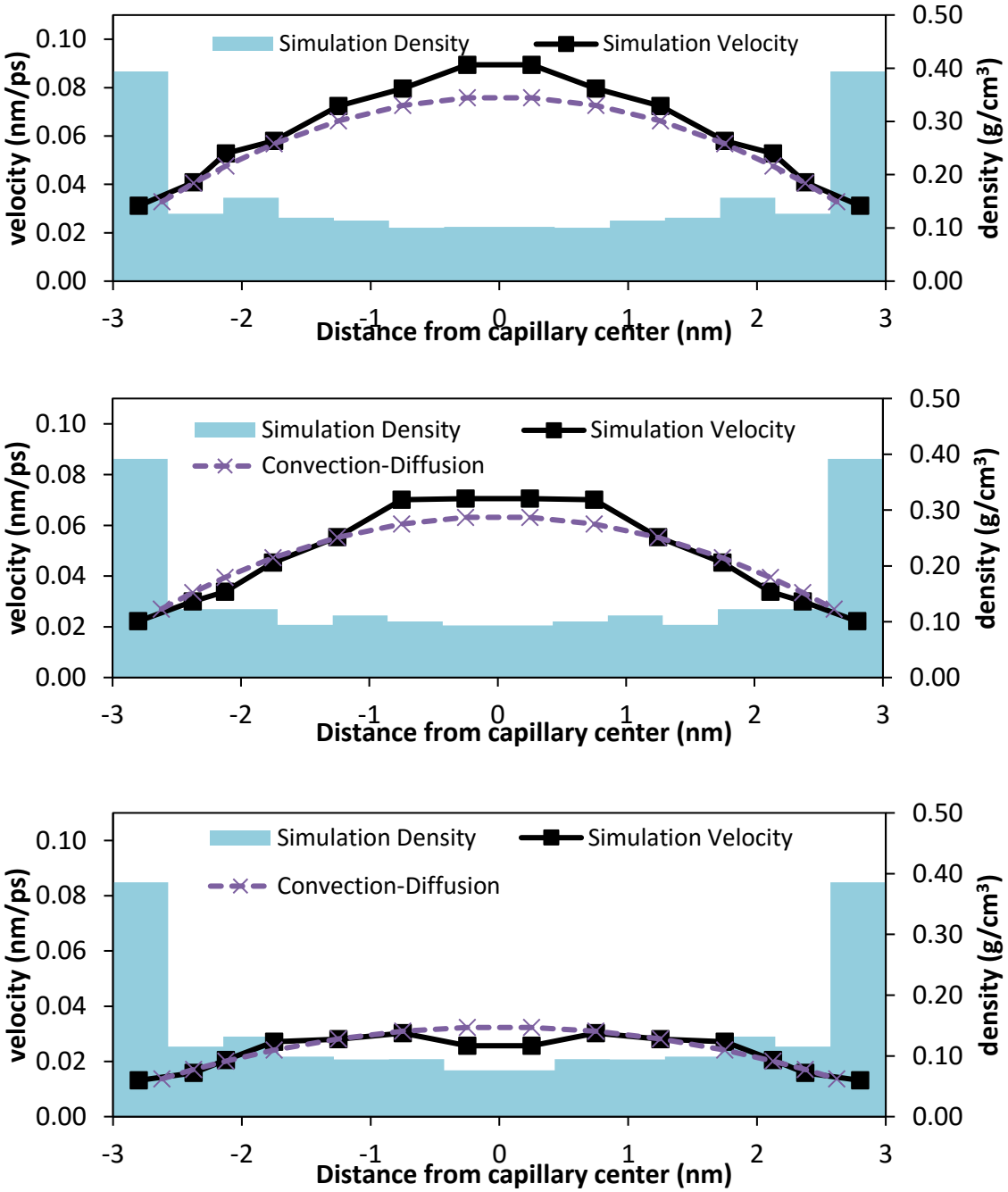


**Figure 14 — Methane velocity profile across the diameter of 6nm capillary at average pressure of 2500psia, temperature of 175 °F (353K). Pressure gradient is: Top: 60psi/nm, Middle: 50psi/nm, and Bottom: 25psi/nm**

Except for viscous flow and Knudsen diffusion, another flow regime that can be identified from the velocity profiles is the adsorbed phase transport right near the capillary walls. In general, in the upstream petroleum industry, the adsorbed phase hydrocarbons are considered immobile. It is assumed that during production the adsorbed hydrocarbons may contribute to total mass flux only when they desorb and become part of the flowing fluid stream. However, our simulation results show that the adsorbed methane molecules have nonzero velocity in the flow direction. This, in turn shifts up the whole velocity profile across the capillary. Figure 13 shows the adsorbed methane is moving at 0.03nm/ps under 65psi/nm pressure gradient. The adsorbed methane moves at 0.02nm/psi under 45psi/nm pressure gradient. The trend of adsorbed phase velocity shows that it is influenced by the pressure gradient applied. The non-zero velocity prevails in both convection-dominated transport regime (Figure 12, Top) and diffusion-dominated regime (Figure 12, Bottom). Considering the high density of the adsorbed phase, it may contribute a substantial amount to the total mass flux.

Before a discussion on the estimated mass flux profiles across the capillary, it is necessary to briefly mention the nature of the adsorbed-phase transport. All the cases shown in Figure 14 indicate that the adsorbed phase velocity is close to Knudsen diffusion velocity. This points out the nature of the adsorbed phase transport could be also diffusive. The analyzed trajectories of methane molecules indicate that the adsorbed-phase transport is cluster diffusion with a particular mechanism known as glide diffusion, which is conceptualized in Figure 15.

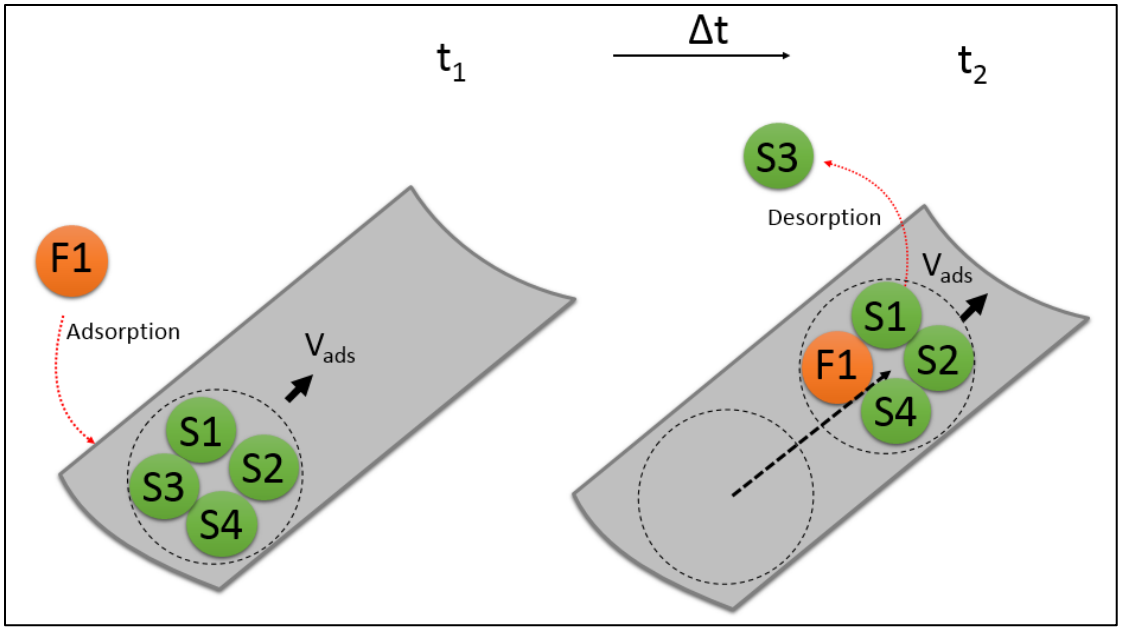


**Figure 15—Diagram of cluster diffusion where methane molecules glide in the direction of main flow in the presence of physical adsorption under equilibrium.**

During glide diffusion, the methane molecules inside the nano-capillary can swap places fast, when an adsorbed molecule (S3) is released and a free molecule (F1) is adsorbed, while the adsorbed phase density maintain unchanged. Hence, transport in the capillary occurs under equilibrium adsorption.

## 3.4 Mass Flux Profile Of Methane In Nanotube

In order to compare mass flux contribution of the adsorbed molecules and the free molecules, we used density and velocity profiles. For each segment across the diameter, the mass flux is represented by the product of the predicted density and velocity for that segment.

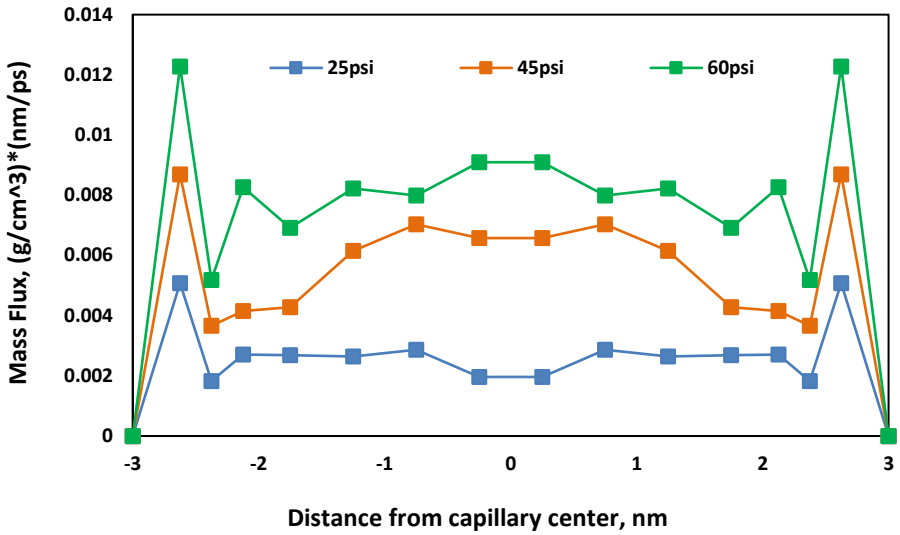


**Figure 16 — Methane mass flux profile during steady-state flow. Varying pressure gradient at average pressure of 2,500 psia, temperature of 175 °F (353 K)**

We plot mass flux across the diameter of capillary at varying pressure gradient in Figure 16. In general, this plot shows mass flux is also dependent on pressure gradient. But, more importantly, the estimated mass fluxes receive peak values near the capillary walls. The peaks represent the presence of large mass flux due to the adsorbed phase transport. In all three pressure gradients cases, due to the high density of adsorbed-phase fluid, even though adsorbed phase velocity is smaller than free phase velocity, its mass flux rate is still larger than free phase. Therefore, when estimating mass flux in nano-capillary, it is necessary to account for mass flux contributed by the adsorbed phase transport. Another observation is, at low pressure gradient, mass flux of free fluid is uniform across the diameter of capillary. This observation confirms our previous result that diffusion is the dominating flow regime at low pressure gradient.

So far we have shown that the actual flow of supercritical methane in organic nano-capillary is a combination of three transport mechanisms: viscous flow (convection), molecular diffusion and adsorbed molecules transport. Using a simple viscous flow model such as HP equation to predict mass flux in nano-capillary will underestimate the total mass flux. Indeed one would argue that the carbon tube walls are smooth, hence, the flow is missing drag forces by the walls. Then the magnitude of the surface heterogeneities, and roughness needs to be considered. To quantify the true mass flux based on HP prediction, Riewchotisakul and Akkutlu (2015) introduced the mass flux ratio as follows:

$$R_{mf} = \frac{Mass\ Flux(total)}{Mass\ Flux(Hagen\ Poiseuille)} = \frac{Density(simulated) \times Velocity(simulated)}{Density(bulk) \times Velocity(Hagen\ Poisseuille)} \quad (35)$$

Here, mass flux ratio, $R_{mf}$, represents the amount of underestimation based on the HP equation. In Figure 17, the predicted mass flux ratio of several flow simulations are presented at a fixed pressure gradient for varying sizes of capillaries. Result shows mass flux in 5 nm diameter capillary is twice larger than that for the HP flow, whereas in the case of 3 nm diameter capillary, mass flux is 5 times larger.

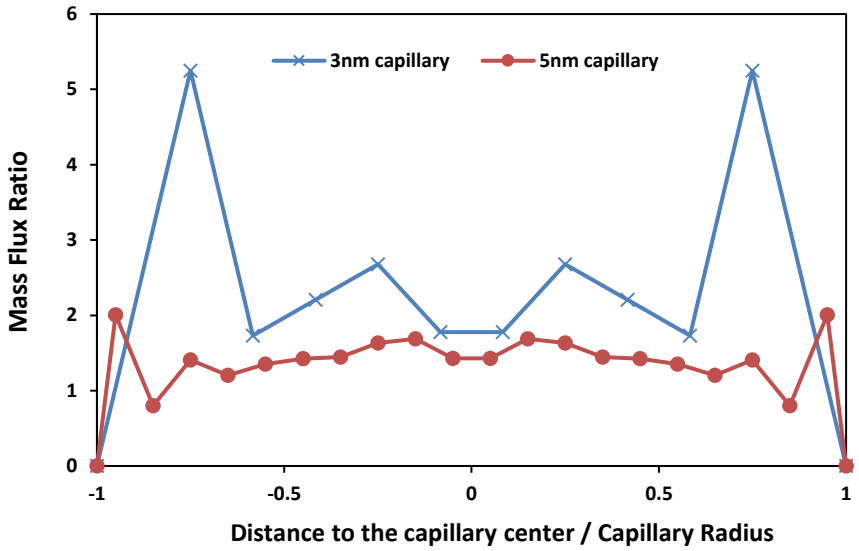


**Figure 17 — Methane mass flux ratio during steady-state flow. At average pressure of 2,500 psia, temperature of 175 °F (353 K), 65psi/nm pressure gradient**

This plot shows that, as the capillary size decreased, the under-estimation of flux using HP equation becomes more significant. This is because the adsorbed molecules take up a larger percentage of capillary space as the capillary size decrease. Hence, in truly nano-porous materials such as kerogen, ignoring the adsorbed-phase transport is expected to lead to a large error in mass flux calculations.

3.5 Adsorbed Phase Mobility

To quantify mass flux contribution of the adsorbed-phase transport, we need to quantify the adsorbed phase velocity in the direction of flow. We run a series of MD simulation with different capillary sizes ranging from 2nm to 6nm, at different pressure gradient. Figure 18 shows relationship between adsorbed phase velocity and pressure gradient, with $R^2$=0.91:

$$V_{ads} = 5\times10^{-4}(dP/dL) - 3\times10^{-4} \quad (36)$$

This observation was originally made by Riewchotisakul and Akkutlu (2015) using a single capillary. Here, based on our simulation results with different size capillaries, we observe that the linear relationship still prevails. Hence, the velocity of the adsorbed molecules is independent of the capillary size and fluid pressure. Therefore, we propose to use the following equation to quantify the adsorbed phase velocity:

$$V_{ads} = D_a \frac{\partial P}{\partial x} \quad (37)$$

where: $V_{ads}$ is adsorbed phase velocity in nm/ps, $D_a$ is adsorbed phase mobility, which equals to $5\times10^{-4}$ $nm^2/(psi \cdot ps)$, $\frac{\partial P}{\partial x}$ is pressure gradient in psi/nm.

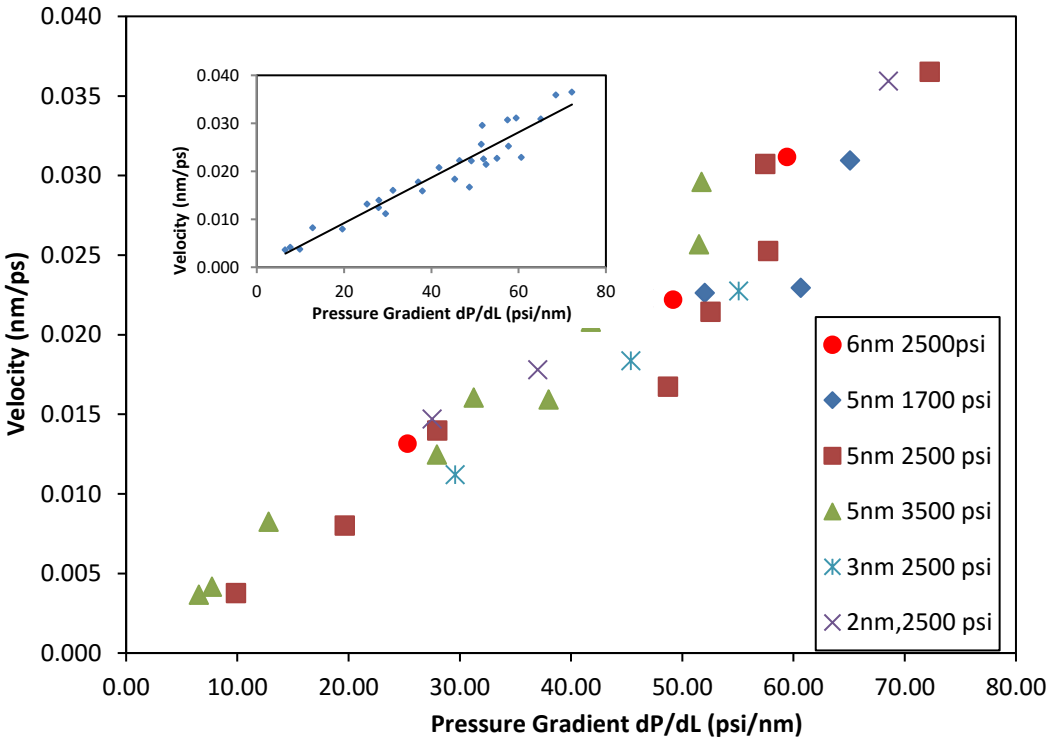


**Figure 18 — Adsorbed-phase methane velocity at varying pressure gradient, varying capillary size and constant temperature of 175 °F (353 K)**

3.6 Mean Free Path And Viscosity

We show that under larger pressure gradient, methane flow in nano capillary has the signature (parabolic shape) of viscous flow. To calculate mass flux contributed by viscous flow, knowledge on fluid viscosity is essential to the calculation. Therefore in this section, we will use MD simulation to estimate viscosity of free fluid and adsorbed fluid in nano capillary. The method we use is based kinetic gas theory illustrated in Section 1.3. Detailed simulation set up can be found in Section 2.3. Here we show the simulation results.

Using algorithm in Section 2.3, we can calculate the time window between two consecutive collisions of a methane molecule. Figure 19 is the statistical distribution of "time between collisions" for free phase methane. It shows time between two collisions ranging from 0 to 3000 fs, with a peak of distribution at 400ps and less. To calculate mean free path, we take the average of this distribution, which is 538 fs.

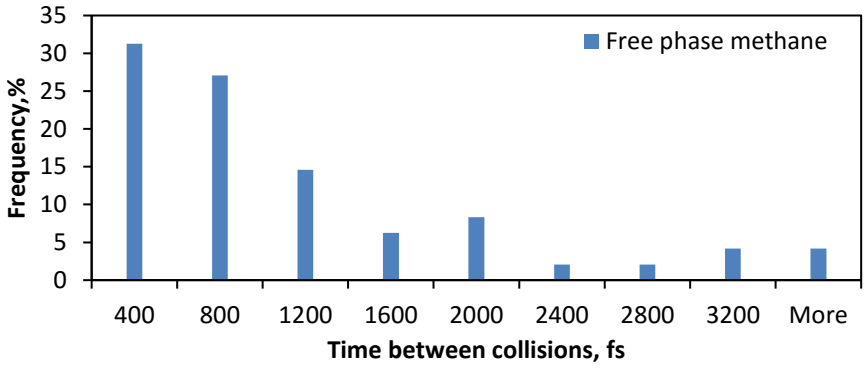


**Figure 19 — free phase methane time between collisions distribution, in femtosecond**

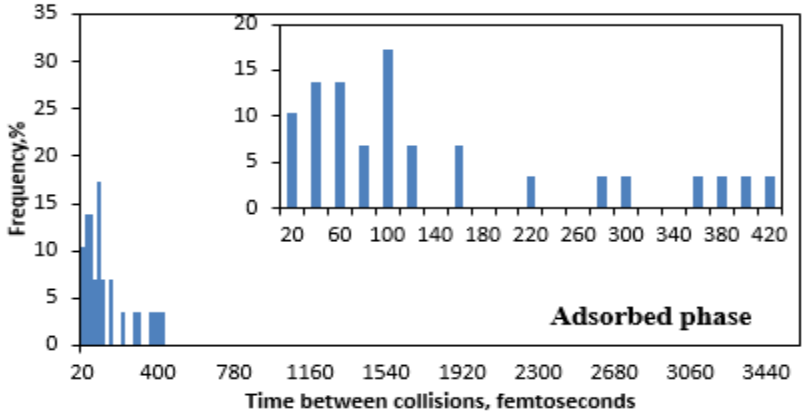


**Figure 20—adsorbed phase methane time between collisions, in femtosecond**

We apply the same algorithm to adsorbed phase fluid, the statistical distribution of "time between collisions" is shown in figure 20.

| Table 2. Free Fluid Mean Free Path and Viscosity | | |
|---|---|---|
| Method | MD simulation | Kinetic Theory |
| Mean Free Path, m | 3.67E-10 | 3.98E-10 |
| Density, kg/m3 | 101.7 | 101.45 |
| Thermal Speed, m/s | 706 | 683 |
| Viscosity, Pa s | 8.79E-06 | 9.19E-06 |

| Table 3. Adsorbed Fluid Mean Free Path and Viscosity | | |
|---|---|---|
| Method | MD simulation | Kinetic Theory |
| Mean Free Path, m | 0.874E-10 | 3.98E-10 |
| Density, kg/m3 | 406.8 | 101.45 |
| Thermal Speed, m/s | 706 | 683 |
| Viscosity, Pa s | 8.37E-06 | 9.19E-06 |

Different from free fluid, the typical range of time between collisions is between 0 to 500fs. And the peak is showing at 100fs and less. The averaged time between collisions is 128 fs. This indicate at adsorbed layer, molecules are colliding with each other with a much higher frequency.

Based on distribution of time between collisions, we can calculate mean free path and viscosity for both free fluid and adsorbed fluid based on equations in Section 1.3. Detailed results are shown in Table 2 and Table 3.

As shown in Table 2, mean free path of free fluid is almost the same as predicted by kinetic theory. Using density and thermal speed value from MD simulation, our final result of viscosity is very close to the value predicted by kinetic theory. This validate our model. Some interesting result are shown in Table 3. The mean free path of adsorbed fluid is much smaller than free fluid. It is about 25% of free fluid mean free path. Besides, density of adsorbed fluid is about 4 times larger than free fluid. However, the changes in mean free path and density didn't influence viscosity. The viscosity of adsorbed fluid is similar to free fluid, which both are close to the value predicted by kinetic theory.

Here we want to inform reader that the method we use to calculate mean free path is purely based on MD simulation, which is not subject to the limitation of kinetic theory of gas. However, to calculate viscosity, we used equations based on kinetic theory of gas, and therefore, the accuracy of viscosity result is limited by the accuracy of kinetic gas theory. To achieve better quantification of viscosity, it is recommended to use advanced theory like kinetic theory for dense gas.

# 4. COMBINED FLOW MODEL

## 4.1 Convection-Diffusion-Adsorbed Phase Transport Equation

In literature review section, we already showed the necessity and application of convection-diffusion equation in describing fluid transport. Given the significance of adsorbed phase transport in organic nano capillary, we propose the following convection-diffusion-surface diffusion equation, where total mass transfer rate consists of convective (or viscos) flow$M_{vis}$, diffusion mass transfer rate$M_{dfs}$, and adsorbed phase mass transfer rate $M_{ads}$.

$$M_{total} = M_{vis} + M_{diff} + M_{ads} \tag{38}$$

To calculate adsorbed phase mass transfer rate, we use adsorbed phase density times adsorbed phase volume flux.

$$M_{ads} = \rho_{ads} Q_{ads} \tag{39}$$

Volume transfer rate can be calculated as adsorbed phase velocity time cross section area of cylindrical capillary

$$Q_{ads} = v_{ads} A_{ads} = v_{ads} \pi (r_{tube}^2 - r_{ads}^2) \tag{40}$$

Adsorbed phase velocity is proportional to pressure gradient

$$V_{ads} = D_{ads} \frac{\partial P}{\partial x} \tag{41}$$

Combining three equations above, we have

$$M_{ads} = \rho_{ads} D_{ads} \pi (r_{tube}^2 - r_{ads}^2) \frac{\partial P}{\partial x} \tag{42}$$

Diffusion mass transfer rate is calculated by molar flux, molecular weight and cross section area

$$M_{diff} = J_{diff} A_{diff} M_{CH4} \tag{43}$$

Diffusion molar flux is calculated by Dick's law

$$J_{diff} = D_{diff} \frac{\partial C}{\partial x} \tag{44}$$

$$\frac{\partial C}{\partial x} = \frac{1}{ZRT} \frac{\partial P}{\partial x} \tag{45}$$

$$J_{dfs} = \frac{1}{ZRT} D_{diff} \frac{\partial P}{\partial x} \tag{46}$$

In the case of multi-component, $c$ is molar concentration of solvent, P is partial pressure of solvent. In the case of single component methane, P is simply gas pressure. In the case of cylindrical 1-D capillary, we have

$$A_{dfs} = \pi r_{tube}^2 \tag{47}$$

$$M_{dfs} = \frac{1}{ZRT} M_{CH4} D_{diff} \pi r_{tube}^2 \frac{\partial P}{\partial x} = \frac{\rho_{bulk}}{P} D_{diff} \pi r_{tube}^2 \frac{\partial P}{\partial x} \tag{48}$$

Convective flow can be calculated using integration of HP equation

$$M_{vis} = \rho_{bulk} Q_{vis} \tag{49}$$

$$Q_{vis} = \frac{\pi r_{ads}^4}{8\mu} \frac{\partial P}{\partial x} \tag{50}$$

Total mass transfer rate is combination of viscos flow, diffusion and adsorbed phase transport.

$$M_{total} = M_{vis} + M_{diff} + M_{ads} \tag{51}$$

We bring in Eq. 38, 44, 45 and 46.

$$M_{total} = \rho_{bulk} \frac{\pi r_{ads}^4}{8\mu} \frac{\partial P}{\partial x} + \frac{\rho_{bulk}}{P} D_{diff}\, \pi\, r_{tube}^2 \frac{\partial P}{\partial x} + \rho_{ads}\, D_{ads} \pi\, (r_{tube}^2 - r_{ads}^2) \frac{\partial P}{\partial x} \quad (52)$$

Equation (52) has 3 terms on the right hand side, each representing mass transfer rate of one transfer mechanism. The fact is this equation can be transform into our classical transport equation by ignoring one or two of the terms under certain conditions. For example, when we consider low pressure gas transport through inorganic capillary, the adsorbed-phase transport term can be ignored. By re-arranging equation, we can show classical Klinkenberg equation is one generalized case of convection-diffusion-surface diffusion equation.

$$M_{total} = 0 + \frac{\rho_{bulk}}{P} D_{diff}\, \pi\, r_{tube}^2 \frac{\partial P}{\partial x} + \rho_{bulk} \frac{\pi r_{tube}^4}{8\mu} \frac{\partial P}{\partial x} \quad (53)$$

$$q = M_{total}/\rho_{bulk} = \frac{1}{P} D_{diff}\, \pi\, r_{tube}^2 \frac{\partial P}{\partial x} + \frac{\pi r_{tube}^4}{8\mu} \frac{\partial P}{\partial x} \quad (54)$$

Bring in k = $r_{tube}^2/8$ , A = $\pi r_{tube}^2$ for a cylindrical capillary

$$q = \frac{1}{P} D_{diff}\, A\, \frac{\partial P}{\partial x} + \frac{kA}{\mu} \frac{\partial P}{\partial x} \quad (55)$$

$$q = \frac{kA}{\mu} \left(1 + \frac{1}{P} \frac{D_{diff}\mu}{k}\right) \frac{\partial P}{\partial x} \quad (56)$$

$$q = \frac{kA}{\mu} \left(1 + \frac{b}{P}\right) \frac{\partial P}{\partial x} \quad (57)$$

Furthermore, if we consider high pressure gas flow through large capillary, both surface diffusion and diffusion terms can be ignored, convection-diffusion-surface diffusion equation simply becomes conventional Darcy's law.

Based on this combined model, we observe that diffusion contribution is sensitive to pressure. This behavior is same as diffusion contribution in Klinkenberg

equation. Convection and adsorbed phase mass transport is sensitive to capillary size. Figure21 (top) shows a clear transition from convection dominated transport (green) to surface diffusion dominated transport (blue) in nano-capillaries under the reservoir condition (high pressure). This is because the thickness of adsorbed phase is constant regardless of capillary size. When capillary size decrease to less than 10 nm, a majority of capillary space is occupied by adsorbed phase.

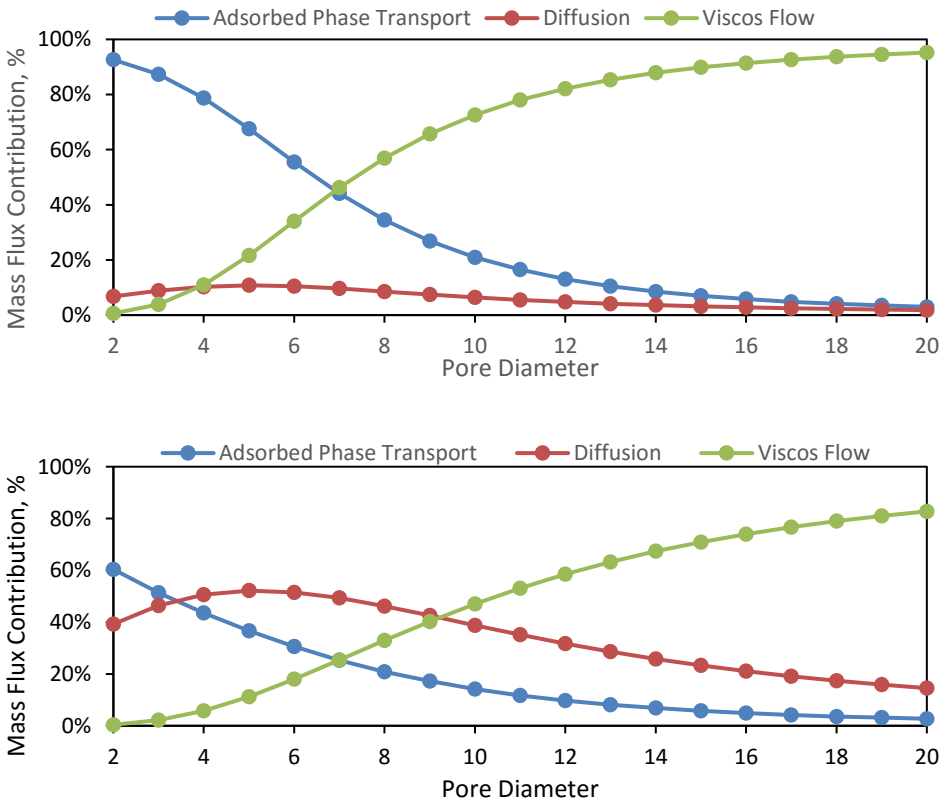


**Figure 21— Mass flux contribution at high pressure of 2500psi (top) versus mass flux contribution at low pressure of 500psi (bottom)**

The contribution of diffusion term is more pronounced at low pressure condition. As shown in Figure 20 (bottom), the diffusion has a significant contribution. These observations are all in line with Klinkenberg equation, which is commonly applied for gas flow in small capillary under low pressure. Different from the intuitive explanation of slip theory, we show here that it is actually the contribution of diffusion that caused the deviation from classical viscos flow theory.

## 4.2 Mass Flux Enhancement Factor

We already showed that convective flow alone is not sufficient to account for total mass flux. To amend for the deficiency that conventional permeability only account for convection flow, one simple way is to apply a correction factor to the existing permeability, which account for the extra flux contributed by other mechanism. We define mass flux enhancement factor as

$$R_{mf} = \frac{M_{total}}{M_{HP}} = \frac{M_{vis}+M_{diff}+M_{ads}}{M_{HP}} \tag{58}$$

Bringing in previous equation for each term, we have

$$R_{mf} = \frac{\rho_{bulk}\frac{\pi r_{ads}^4}{8\mu}\frac{\partial P}{\partial x}+\frac{\rho_{bulk}}{P}D_{diff}\,\pi\, r_{tube}^2\frac{\partial P}{\partial x}+\rho_{ads}\,D_{ads}\pi\left(r_{tube}^2-r_{ads}^2\right)\frac{\partial P}{\partial x}}{\rho_{bulk}\frac{\pi r_{tube}^4}{8\mu}\frac{\partial P}{\partial x}} \tag{59}$$

Separate convection term

$$R_{mf} = \frac{\rho_{ads}\,D_{ads}\pi\left(r_{tube}^2-r_{ads}^2\right)+\frac{\rho_{bulk}}{P}D_{diff}\,\pi\, r_{tube}^2}{\rho_{bulk}\frac{\pi r_{tube}^4}{8\mu}} + \frac{r_{ads}^4}{r_{tube}^4} \tag{60}$$

$$R_{mf} = 8\mu[\frac{\rho_{ads}}{\rho_{bulk}} \frac{D_{ads}}{r_{tube}^2} \frac{(r_{tube}^2 - r_{ads}^2)}{r_{tube}^2} + \frac{1}{P} \frac{D_{diff}}{r_{tube}^2}\ ] + \frac{r_{ads}^4}{r_{tube}^4} \quad (61)$$

Separate diffusion and surface diffusion term, we have the final form of $R_{mf}$ equation:

$$R_{mf} = \frac{r_{ads}^4}{r_{tube}^4} + 8\mu \frac{1}{P} \frac{D_{diff}}{r_{tube}^2} + 8\mu \frac{\rho_{ads}}{\rho_{bulk}} \frac{D_{ads}}{r_{tube}^2} \frac{(r_{tube}^2 - r_{ads}^2)}{r_{tube}^2} \quad (62)$$

Final form is mass flux enhancement factor consist of three terms, corresponding to surface diffusion, diffusion and convection flow. It is dependent on both capillary size and pressure. At high pressure (between 2000psi and 5000psi), influence of pressure change on Rme is minimum because only diffusion term inversely proportional to pressure. We plot mass transport enhancement factor by equation and by MD simulation as below.

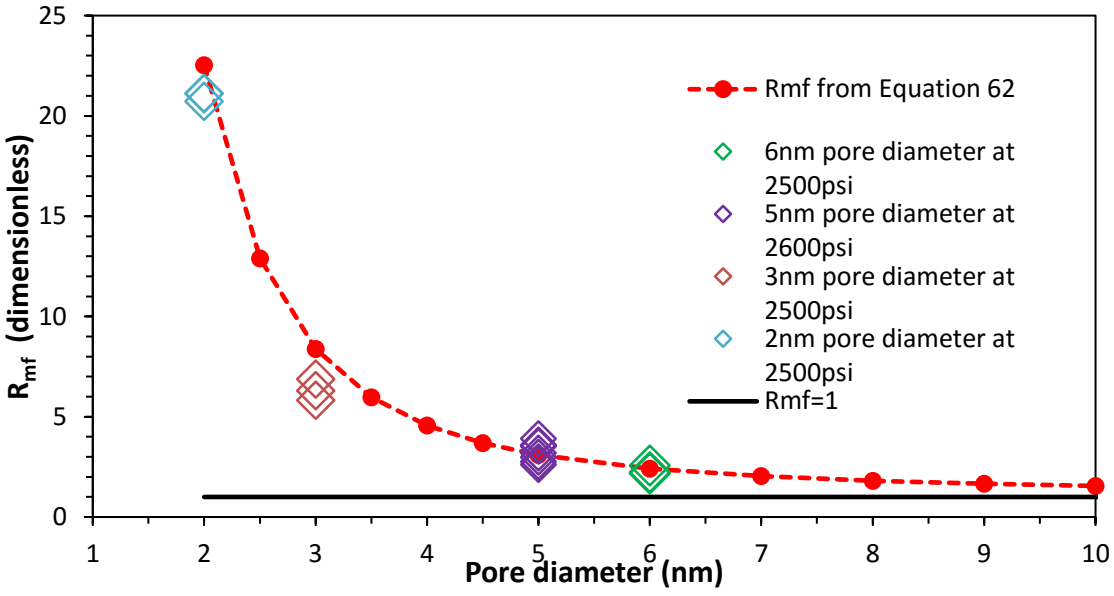


**Figure 22— Mass Flux Ratio Calculated versus mass flux ratio simulated, with pore diameter ranging from 2-15 nm**

Mass flux ratio predicted by the analytical expression above and from molecular dynamics simulation match. As capillary diameter decreases, mass flux ratio increases, which indicates the necessity to correct mass flux for small pores. On the other hand, for pore diameter larger than 10nm, $R_{mf}$ value almost equal to 1. This means for large capillaries (diameter >10nm), mass flux contributed by diffusion and adsorbed phase transport is overwhelmed by mass flux by viscos flow, making convection the dominant flow regime.

## 4.3 Apparent Permeability Model

Using same convection-diffusion-surface diffusion equation, we can calculate apparent permeability, where total mass flux is combination of three mechanism:

$$J_{total} = J_{vis} + J_{diff} + J_{ads} \tag{63}$$

Each of the flow mechanism can be calculated as:

$$J_{vis} = \rho \frac{k_m}{\mu} \frac{\partial P}{\partial x} \tag{64}$$

$$J_{diff} = M_w D_{diff} \frac{\partial C}{\partial x} = M_w \frac{D_{dfs}}{ZRT} \frac{\partial P}{\partial x} \tag{65}$$

$$J_{ads} = \frac{(r_{tube}^2 - r_{ads}^2)}{r_{tube}^2} \rho_{ads} * V_{ads} = \frac{(r_{tube}^2 - r_{ads}^2)}{r_{tube}^2} \rho_{ads} * D_{ads} \frac{\partial P}{\partial x} \tag{66}$$

Substitute all three equations into Equation 63

$$J_{total} = \rho \frac{k_m}{\mu} \frac{\partial P}{\partial x} + M_w \frac{D_{diff}}{ZRT} \frac{\partial P}{\partial x} + \frac{(r_{tube}^2 - r_{ads}^2)}{r_{tube}^2} \rho_{ads} * D_{ads} \frac{\partial P}{\partial x} \tag{67}$$

Final form is

$$J_{total} = \rho \frac{k_m}{\mu} \frac{\partial P}{\partial x} + \frac{\rho}{P} D_{diff} \frac{\partial P}{\partial x} + \frac{(r_{tube}^2 - r_{ads}^2)}{r_{tube}^2} \rho_{ads} D_{ads} \frac{\partial P}{\partial x} \quad (68)$$

We define apparent permeability in the following equation

$$J_{total} = \rho \frac{k_a}{\mu} \frac{\partial P}{\partial x} \quad (69)$$

Combine Eq 68 and 69, we have apparent permeability as below

$$k_a = k_m + \mu \frac{D_{diff}}{P} + \frac{(r_{tube}^2 - r_{ads}^2)}{r_{tube}^2} \mu \frac{\rho_{ads}}{\rho} * D_{ads} \quad (70)$$

Again, the apparent permeability equation contains three terms, representing permeability contributions by viscous flow, by diffusion and by the adsorbed phase transport, respectively. Diffusion's contribution to permeability is proportional to the inverse of pressure. The adsorbed molecules contribution to the permeability is dependent on the magnitude of the adsorbed phase mobility $D_{ads}$. as well as the density contrast $\frac{\rho_{ads}}{\rho}$.

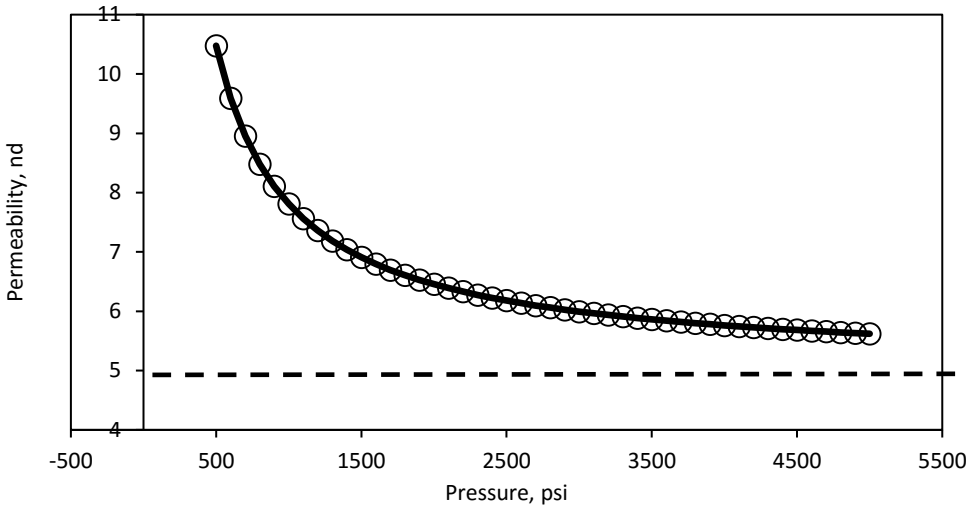


**Figure 23— Apparent permeability calculation based on 5nd matrix permeability, 10nm equivalent pore diameter.**

We plot the apparent permeability dependence in the pore pressure in Figure 23. Note that the second and third terms are pressure dependent. For the purpose, we considered 10nm equivalent pore diameter with rough surfaces. This capillary should have $k$=5md based on HP flow. As shown in Figure 23, at low pressure, the apparent permeability increases due to mass flux contribution from molecular diffusion and adsorbed phase transport. These results are indicating that the apparent permeability could also be sensitive to the composition of the fluid. Wasaki and Akkutlu (2015a) observed similar apparent permeability behavior due to molecular transport, they further point out the apparent matrix permeability ($k_a$) is sensitive to effective stress, consequently could decrease with the pore pressure Wasaki and Akkutlu (2015a,b). These sensitivity effects are dominant at large pores, micro-cracks and are not likely to influence the kerogen permeability.

# 5. CONCLUSION

This research start from the Monte-Carlo equilibrium simulation of methane gas in slit shape organic pores. Result of simulation shows heterogeneity in gas density distribution. With the ratio of adsorbed phase density to bulk phase density quantified, we move on to Molecular Dynamics simulation to investigate flow regime in kerogen capillary. In MD simulation, we build a piston model which are able to simulation steady-state gas flow in carbon nano-tube. From velocity profile and mass flux profile, we identified three flow mechanism that contributes to the total mass flux, which are viscous flow, diffusion and surface diffusion.

Based on Convection-Diffusion-Adsorbed model, we investigate how pore size and pressure influence apparent permeability, and applied the result to apparent permeability estimation of shale rock. As shown in the apparent permeability plot, at low pressure contributions of diffusion flux is getting pronounced and enhancing apparent permeability of shale rock. Research of fracture conductivity influence near wellbore pressure distribution (Wasaki, Akkutlu 2015) shows that maintaining infinite fracture conductivity will result in lower pressure in near wellbore region. Combining our apparent permeability model, it is desirable to maintain high fracture conductivity of hydraulic fracturing, so that to achieve lower near wellbore pressure distribution and higher apparent permeability.

To quantify contribution of diffusion at low pressure more rigorously, it is recommended to measure diffusion coefficient of shale samples from specific shale play using fluid representing reservoir components. Limited by currently experiment capacity, it is equally desirable to have simulated diffusion coefficient using digital rock model based on pore size distribution. Further research work can be done in these experimental and simulation areas.

# REFERENCES


1. Ambrose, R.J., Hartman, R.C., Diaz-Campos, M., Akkutlu, I.Y., And Sondergeld, C.H. 2012. Shale Gas In-Place Calculations Part I - New Pore-Scale Considerations. SPE Journal. Volume 17 (1) 219-229

2. Akkutlu, I.Y. And Fathi E. 2012. Multi-Scale Gas Transport In Shales With Local Kerogen Heterogeneities. SPE Journal, Volume 17 (4), 1002-1011.

3. Beskok, A., Karniadakis, G.E., 1999. A Model For Flows In Channels, Pipes And Ducts At Micro And Nano Scales. Microscale Thermophys Eng., 3(1):43-77

4. Civan. F., 2010. Effective Correlation Of Apparent Gas Permeability In Tight Porous Media. Transport In Porous Media, 82: 375-384

5. Cristancho, D.A., Akkutlu, I.Y., Criscenti, L. And Wang, Y. 2016. Gas Storage In Model Kerogen Pores With Surface Heterogeneities. SPE-180142 To Be Presented At The SPE EUROPEC Featured At 78th EAGE Conference And Exhibition, Vienna, Austria 30 May-2 June.

6. Fathi E. And Akkutlu, I.Y. 2012. Mass Transport Of Adsorbed-Phase In Stochastic Porous Medium With Fluctuating Porosity Field And Nonlinear Gas Adsorption Kinetics. Journal Of Transport In Porous Media, Volume 91 (1) 5-33.

7. Feng, F. And Akkutlu, I.Y. 2015. Flow Of Hydrocarbons In Nanocapillary: A Non-Equilibrium Molecular Dynamics Study. SPE-177005, Paper Presented At The SPE Asia Pacific Unconventional Resources And Exhibition Held In Brisbane, Australia, November 9-11.

8. Gangi, A. F. 1978. Variation Of Whole And Factured Porous Rock Permeability With Confining Pressure, International Journal Of Rock Mechanics And Mining Secinces & Geomechanics Abstracts, Volume 15(5), 249-257

9. Gagnon, Marc-André, and Michel Lafleur. "Self-diffusion and mutual diffusion of small molecules in high-set curdlan hydrogels studied by 31P NMR." The Journal of Physical Chemistry B 113.27 (2009): 9084-9091.

10. Javadpour, F. (2009). Nanopores And Apparent Permeability Of Gas Flow In Mudrocks (Shales And Siltstone). Petroleum Society Of Canada. Doi:10.2118/09-08-16-DA

11. Kang S., Fathi, E., Ambrose, R.J., Akkutlu, I.Y., And Sigal, R.F. 2011. Carbon Dioxide Storage Capacity Of Organic-Rich Shales. SPE Journal, Volume 16 (4), 842-855

12. Karniadakis, G.E. Beskok,A. Alluru, N. 2005. Microflows And Nanoflows Fundamentals And Simulation. Volume 29

13. Kellogg, Gary L. "Field ion microscope studies of single-atom surface diffusion and cluster nucleation on metal surfaces." Surface Science Reports 21.1-2 (1994): 1-88.

14. Loucks, R. G., R. M. Reed, S. C. Ruppel, And D. M. Jarvie, 2009, Morphology, Genesis, And Distribution Of Nanometer-Scale Pores In Siliceous Mudstones Of The Mississippian Barnett Shale: Journal Of Sedimentary Research, V. 79, P. 848–861, Doi:10.2110/Jsr.2009.092

15. Michely, Thomas, et al. "Inversion of growth speed anisotropy in two dimensions." Physical review letters 70.25 (1993): 3943.

16. O'Carroll, C., & Sorbie, S. 1993. Generalization Of The Poiseuille Law For One- And Two-Phase Flow In A Random Capillary Network. Physical Review E, 47:5, 3467-3476

17. Palciauskas V. V., Domenico P. A.. 1980. Microfracture Development In Compacting Sediments: Relation To Hydrocarbon-Maturation Kinetics AAPG Bulletin, Volume 64(6) 927-937

18. Prabha, Sooraj K., P. D. Sreehari, and Sarith P. Sathian. "The effect of system boundaries on the mean free path for confined gases." AIP Advances 3.10 (2013): 102107.

19. Rahmanian M., Aguilera, R., Kantzas, A. 2013. A New Unified Diffusion-Viscous – Flow Model Based On Pore Level Studies Of Tight Gas Formations. SPE Journal:38-49

20. Riewchotisakul, S. And Akkutlu, I.Y. 2015. Adsorption–Enhanced Transport Of Hydrocarbons In Nanometer-Scale Organic Pores. SPE-175107, Paper Presented During The SPE Annual Technical Conference And Exhibition In Houston, Texas, September 28

21. Sakhaee-Pour, A. Bryant, S. 2012. Gas Permeability Of Shale. SPE Reservoir Evaluation & Engineering 15 (04): 401–409.. . Doi:10.2118/146944-PA.

22. Singh, H., Javadpour, F., Ettehadtavakkol, A., & Darabi, H. (2014, August 1). Nonempirical Apparent Permeability Of Shale. Society Of Petroleum Engineers. Doi:10.2118/170243-PA

23. Soto, J. L., and A. L. Myers. "Monte Carlo studies of adsorption in molecular sieves." Molecular Physics 42.4 (1981): 971-983.

24. Thomas J.A. And Mcgaughey, A.J.H. 2009. Water Flow In Carbon Nanotubes: Transition To Subcontinuum Transport. Physical Review Letters **102** (18) 184502(4)

25. Wang, F.P. And Reed, R.M. 2009. Pore Networks And Fluid Flow In Gas Shales. Paper SPE 124253 Presented At The SPE Annual Technical Conference And Exhibition, New Orleans, 4-7 October.

26. Wasaki, A. And Akkutlu, I.Y. 2015a. Permeability Of Organic-Rich Shale. SPE Journal, Volume 20 (6), 1384-1396.

27. Wasaki, A., And Akkutlu, I. Y. 2015b. Dynamics Of Fracture-Matrix Coupling During Shale Gas Production: Pore Compressibility And Molecular Transport Effects. Society Of Petroleum Engineers. Doi:10.2118/175033-MS

28. Woods, Gary B., and John S. Rowlinson. "Computer simulations of fluids in zeolites X and Y." Journal of the Chemical Society, Faraday Transactions 2: Molecular and Chemical Physics 85.6 (1989): 765-781.